Article

Secondary organic aerosol formation from healthy and aphid-stressed Scots pine emissions

Celia Faiola, Iida Pullinen, Angela Buchholz, Farzaneh Khalaj, Arttu Ylisirniö, Eetu Kari, Pasi Miettinen, Jarmo K. Holopainen, Minna Kivimäenpää, Siegfried Schobesberger, Taina Yli-Juuti, and Annele Virtanen

Just Accepted

Secondary Organic Aerosol Formation from Healthy and Aphid-Stressed Scots Pine Emissions

Authors: Celia L. Faiola[1,2*], Iida Pullinen[3], Angela Buchholz[3], Farzaneh Khalaj[1], Arttu Ylisirniö[3], Eetu Kari[3], Pasi Miettinen[3], Jarmo K. Holopainen[4], Minna Kivimäenpää[4], Siegfried Schobesberger[3], Taina Yli-Juuti[3], and Annele Virtanen[3]

[1]Department of Ecology and Evolutionary Biology, University of California Irvine, Irvine, CA, USA, 92697

[2]Department of Chemistry, University of California Irvine, Irvine, CA, USA 92697

[3]Department of Applied Physics, University of Eastern Finland, P.O. Box 1626, 70211 Kuopio, Finland

[4]Department of Environmental and Biological Sciences, University of Eastern Finland, P.O. Box 1627, 70211 Kuopio, Finland

*corresponding author, cfaiola@uci.edu

ABSTRACT:

One barrier to predicting biogenic secondary organic aerosol (SOA) formation in a changing climate can be attributed to the complex nature of plant volatile emissions. Plant volatile emissions are dynamic over space and time, and change in response to environmental stressors. This study investigated SOA production from emissions of healthy and aphid-stressed Scots pine saplings via dark ozonolysis and photooxidation chemistry. Laboratory experiments using a batch reaction chamber were used to investigate SOA production from different plant volatile mixtures. The volatile mixture from healthy plants included monoterpenes, aromatics, and a small amount of sesquiterpenes. The biggest change in the volatile mixture for aphid-stressed plants was a large increase (from 1.4 to 7.9 ppb) in sesquiterpenes—particularly acyclic sesquiterpenes, such as the farnesene isomers. Acyclic sesquiterpenes had different effects on SOA production depending on the chemical mechanism. Farnesenes suppressed SOA formation from ozonolysis with a 9.7-14.6% SOA mass yield from healthy plant emissions and a 6.9-10.4%

SOA mass yield from aphid-stressed plant emissions. Ozonolysis of volatile mixtures containing more farnesenes promoted fragmentation reactions, which produced higher volatility oxidation products. In contrast, plant volatile mixtures containing more farnesenes did not appreciably change SOA production from photooxidation. SOA mass yields ranged from 10.8-23.2% from healthy plant emissions and 17.8-26.8% for aphid-stressed plant emissions. This study highlights the potential importance of acyclic terpene chemistry in a future climate regime with an increased presence of plant stress volatiles.

Keywords: secondary organic aerosol, volatile organic compounds, atmospheric chemistry, plant stress, acetate-CIMS

1. INTRODUCTION

Globally, plant volatile emissions are the largest contributor to secondary organic aerosol (SOA) production[1]. SOA plays an important role in Earth's radiation budget by directly absorbing and scattering light and contributing to cloud formation processes[2]. Plants emit a wide variety of volatile organic compounds (VOCs) with over 1,700 different compounds identified in over ninety plant families[3]. Major classes of VOCs include the terpenoids (i.e. isoprene, monoterpenes, sesquiterpenes, diterpenes, homoterpenes), benzenoids and phenylpropanoids (i.e. methyl salicylate, benzaldehyde, eugenol), and plant stress compounds derived via the lipoxygenase (LOX) pathway (i.e. green leaf volatiles, methyl jasmonate)[4]. Terpenoids are the dominant class of volatiles emitted by plant volatiles with isoprene alone contributing 70% of total global biogenic emissions by mass, followed by monoterpenes at 11%, methanol at 6%, acetone at 3%, sesquiterpenes at 2.5% and all others contributing less than 2%[5]. For this reason, studies of SOA formation chemistry have focused primarily on isoprene and a few of the most prominent monoterpenes (i.e. α-pinene, β-pinene, limonene, and 3-carene)[6,7]. Studies using simplified chemical systems have provided valuable mechanistic insight of SOA formation chemistry. However, plant VOC emission rates and the types of volatiles they emit, change substantially under conditions of plant stress[8–12], and thus the SOA formation chemistry from stressed plant volatiles could look very different in the future under different climate regimes. Boreal forest trees have already exhibited increased plant stress due to earlier onset of spring, warmer summer temperatures, drought, and increased frequency and severity of insect

outbreaks[13–15]. There are very few studies looking at SOA formation from more realistic

mixtures of plant volatiles, and furthermore, how that SOA formation chemistry could change as

the types of volatiles emitted by plants evolves in a changing climate. This study addresses this

important gap by investigating SOA formation chemistry from healthy and stressed Scots pine

emissions, and comparing the results to SOA generated from a well-studied monoterpene

compound, α-pinene.

Under baseline conditions, plant VOC emission rates are largely controlled by abiotic

environmental factors such as light and/or temperature. These are the two dominant variables

modulating emissions in the most widely-used plant emissions model, the Model of Emissions of

Gases and Aerosols from Nature (MEGAN)[16]. However, plant volatile emission rates can

drastically increase during periods of stress, including stress caused by insect herbivores feeding

on plant tissues[17–24]. The degree to which insect herbivory increases emission rates is dependent

on the degree of damage[10]. Furthermore, the types of compounds induced or elevated by the

herbivory stress can vary substantially depending on the type of herbivore. For example, bark-

boring insects feeding on conifer plants will expose the plant's oleoresin storage pools to the

atmosphere, and cause large emission increases in the major terpenes stored in those pools[17]. In

contrast, leaf- (or needle-) eating defoliators cause substantial damage to green plant tissues and

will induce bursts of green leaf volatile emissions - including six-carbon alcohols, aldehydes, and

esters[25,26]. These green leaf volatile compounds are formed from the degradation products of

damaged cell membranes[4]. Finally, piercing-sucking insects (such as the aphids used in this

experiment) induce biochemical metabolic pathways that produce emissions of methyl

salicylate[18]. All these types of insect herbivory can also change the emission profile of the

dominant monoterpenes and sesquiterpenes. For example, a plant hormone treatment that

simulated herbivore stress not only increased total monoterpene emissions from western

redcedar, but also transitioned the monoterpene emission profile from being dominated by β-

phellandrene, β-pinene, and camphene to being dominated by terpinolene[27]. Thus, insect

herbivory has the potential to substantially alter SOA formation chemistry from plant volatiles.

This herbivory effect on SOA formation could be particularly important in the boreal forest

where climate warming has been increasing the extent and frequency of insect outbreaks[28,29], and

where this trend is expected to continue in the future[30].

Insect outbreaks are widespread during spring and summer months[31], so herbivory emissions and SOA formation from those emissions could be important contributors to SOA production. One estimate suggests that plant volatile emissions induced by insect herbivory could account for up to 50% of all organic aerosol mass in Europe[32]. Consequently, an improved understanding of the chemical mechanisms responsible for generating SOA from herbivore-enhanced plant volatile emissions would be useful for predicting organic aerosol mass loadings in the atmosphere. Plant stress from insect herbivory can increase SOA production by increasing plant volatile emission rates[26,33]. This mechanism of increased SOA production also occurs with plants exposed to elevated temperatures[34]. Of particular interest, changes to the plant volatile emission profile (as opposed to total emission rates) can also increase[35] or decrease[17] SOA mass yields, depending on the type of herbivore and how it affects the types of compounds emitted by the plants. For example, when aphid-herbivory stress was combined with heat and drought stress, sesquiterpene and methyl salicylate emissions increased with a measurable increase in SOA mass yields from photooxidation of plant emissions[35]. Importantly, an increase in sesquiterpene contribution to SOA production following aphid herbivory caused a reduction in particle hygroscopicity (from $\kappa=0.15$ for unstressed plants to $\kappa=0.07$ for aphid-stressed plants)[36]—demonstrating that the herbivore stress volatiles can affect climate-relevant properties of the aerosol. In contrast, pine weevil herbivory stress (a bark-boring insect) substantially reduced the sesquiterpene-to-monoterpene ratio of Scots pine volatile emissions and approximately halved the SOA mass yields from photooxidation during active feeding[27]. These contrasting results highlight the importance of studying different herbivore-plant combinations because the herbivory effect on plant volatiles will vary. Furthermore, SOA mass yields vary substantially depending on the oxidation mechanism. For example, SOA mass yields from photooxidation of some major monoterpenes are β-pinene>α-pinene>limonene while the SOA mass yields from ozonolysis are limonene> α-pinene>β-pinene[37]. To our knowledge, SOA experiments using real plant volatile emissions have focused on photooxidation chemistry, and there have been no studies of ozonolysis oxidation.

The objective of this study was to investigate photooxidation and ozonolysis chemistry of a complex mixture of real plant volatiles from Scots pines under healthy and aphid-stressed conditions. To compare our results with previously published data, SOA experiments were also conducted from α-pinene oxidation. To make comparisons across chemical systems, we

characterized the initial VOC profile in each experiment and compared gas-phase oxidation products and SOA mass yields. This is the first report of oxidation products and their estimated volatility distributions from laboratory chamber experiments using healthy and stressed plant volatile emissions.

2. EXPERIMENTAL AND COMPUTATIONAL METHODS

2.1. Plant Description and Plant Volatile Collection

Plant volatiles for the SOA experiments were collected from 8-year old Scots pine (*Pinus sylvestris L.*) saplings. Pinaceae is one of the most widely distributed conifer tree species in the world[38] making up 65% of forested area in Finland[39]. Scots pine geographical range covers Eurasian conifer forests from Scotland to Eastern Siberia close to the Pacific Ocean and south to Turkey. This makes Scots pine emissions a highly representative conifer species for studying chemistry of boreal forest plant emissions. Plants were grown in 7.5-liter pots in a 1:1:1 mixture of quartz sand, garden soil and natural peat in the Kuopio campus research garden field site at the University of Eastern Finland (UEF). Plants received fertilizer treatment (0.5 L of 0.1% fertilizer solution Turve-superex, N:P:K 12:5:27, Kekkilä Oy, Vantaa, Finland) once per week. Saplings for SOA experiments were transported from the field site on May 3rd, 2016 and unstressed control trees were taken to greenhouse in natural long-day conditions 17h daylight (5:00 to 22:00), but warmer conditions (temperature +22°C at day and +12 °C at night) to advance bud-opening and shoot growth. Sapling for stress-treatment were allowed to start their growth in natural conditions with average daily high 14.1 and 18.9 and average daily low 4.3 and 10.3 °C temperatures in May and June, respectively. Four healthy Scots pine saplings were transported to the laboratory on May 31st, 2016 and stored under a high intensity LED grow lamp Valoya B100 DIM NS1 (Valoya Oy, Helsinki, Finland) set on a timer to provide 12 hours of direct light each day. Total hours of light was longer than 12 hours because natural sunlight entered the laboratory from windows with ~20 hours of sunlight in June and July during the summer. The same four saplings were used for all healthy plant SOA experiments. Four different aphid-stressed saplings were transported to the laboratory on July 4th, 2016. All aphid-stressed SOA experiments were performed using emissions from the same set of four plants. Large pine aphid *Cinara pinea* Mord. (Hemiptera: Aphidoidea) that feed and form colonies on pine branch bark and on developing new shoots were used as a stressor insect. Aphids were reared from over-wintering

eggs in growth chambers, and tree branches of stressed sapling were infected on May 22, June 8 and June 21 to achieve strong aphid population (159±57 living aphids per seedling) before transfer to SOA experiments.

While plants were in the lab, a dynamic plant enclosure was installed on each plant. The enclosures were composed of ~70 liter custom-made Tedlar bags (Jensen Inert Products, Inc.) and secured to the plant trunks using cable ties. Each plant enclosure was continuously flushed with 1 L min^{-1} humidified clean air. Clean air was generated from filtered compressed house air. Plants were allowed to acclimate to laboratory conditions in the enclosure for a minimum of 24 hours before any VOCs were collected to avoid capturing any stress VOCs that result from enclosure installation[40,41]. Relative humidity inside the enclosures ranged from 50-70%. The temperature inside the enclosure was monitored with thermocouples and ranged from 23-27 °C throughout the experiment period. Plant volatiles were collected on stainless steel multi-bed adsorbent cartridges containing Tenax TA and Carbograph adsorbent (Markes International, Inc.) by pulling .3-.5 L min^{-1} enclosure air from each enclosure through two cartridges placed in series for 17-20 hours with a vacuum pump. Flows for each collection line were controlled with needle valves (Swagelok, Inc.) and measured with a DryCal Defender 520 (Mesa Labs, Inc.).Tenax and Carbograph adsorbents efficiently trap terpenoids, methyl salicylate, and smaller C_6 green leaf volatiles that are commonly associated with herbivore stress. Cartridges were stored in a refrigerator until they were used for SOA experiments. Importantly, the goal was not to use these cartridges to quantify emission rates from the plant enclosures. The goal was to trap enough volatiles from the plant enclosures for transport to the environmental chamber via thermo-desorption in order to run the SOA chemistry experiments. This long trapping time is the reason two cartridges were placed in series on each enclosure; the downstream cartridge, or "breakthrough" cartridge, would trap volatiles that escaped from the front cartridge. Breakthrough volume for limonene on Tenax TA adsorbent at 20 °C is 13,000 L per gram adsorbent (https://www.sisweb.com/index/referenc/tenaxta.htm). The volume of air we pulled through the cartridges ranged from 300-600 L. For adsorbent cartridges with 100 mg of adsorbent, breakthrough volume through two cartridges in series would be 2,600 L, suggesting we were well below the breakthrough volume.

2.2.   *Oxidation of Plant Volatiles and SOA Production*

Figure 1 shows a schematic of the experimental set-up. SOA experiments were conducted using three different types of VOC precursors: 1) healthy Scots pine emissions, 2) aphid-stressed Scots pine emissions, and 3) α-pinene. Healthy and aphid-stressed Scots pine emissions used for the SOA experiments were trapped on multi-bed adsorbent cartridges as described in Section 2.1 and introduced to the batch reaction chamber via thermo-desorption. VOCs were oxidized in a 9 m^3 Teflon environmental chamber located in a temperature-controlled room at the University of Eastern Finland (Kuopio, Finland). Before each experiment, the chamber was prepared by flushing with clean air overnight. The morning of an experiment, the chamber was adjusted to 50% relative humidity with dry and humidified input flows. The scanning mobility particle sizer (SMPS; TSI, Inc.), high resolution aerosol mass spectrometer (AMS; Aerodyne, Inc.), proton-transfer-reaction time-of-flight mass spectrometer (PTR-ToF-MS; Ionicon, Inc.), and acetate chemical ionization mass spectrometer (CIMS; Aerodyne, Inc.) were turned on to begin
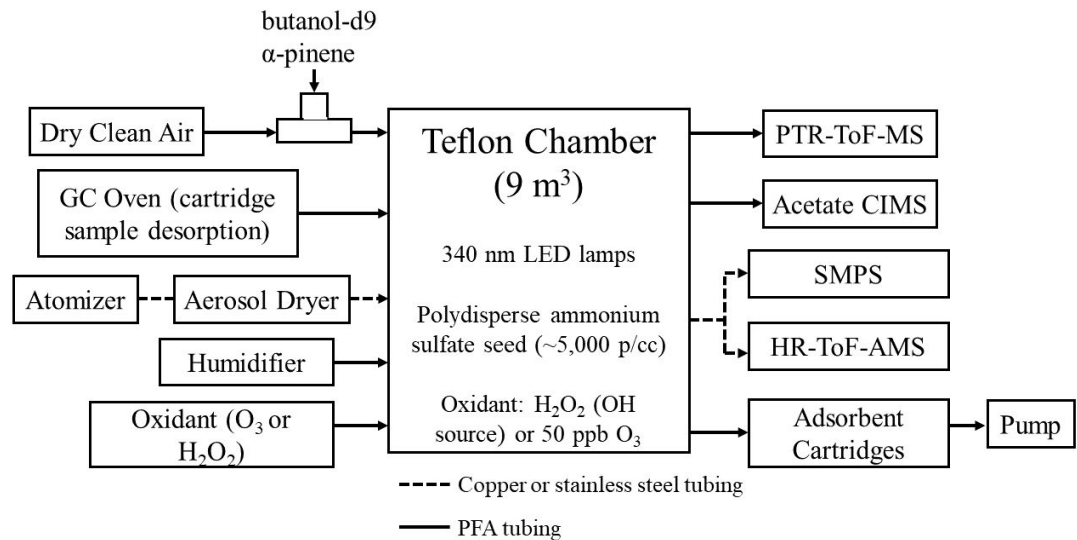
Figure 1: A schematic of the environmental chamber set-up used to conduct the experiments. Plant enclosures, from which plant volatiles were trapped onto adsorbent cartridges, were operated independently from the batch reaction chamber. The plant volatiles were introduced to the Teflon batch reaction chamber via thermo-desorption using the GC oven shown in the schematic.

sampling and verify the chamber was clean. A more detailed description of the instrumentation and their operation is provided in the following section.

Two different oxidation mechanisms were investigated during this study: dark ozonolysis and photooxidation. Experimental procedure differed slightly at this point depending on the oxidation mechanism. For photooxidation experiments, 3.5 mL H_2O_2-solution (30% w/v in water, Fisher Scientific UK Ltd.) was added to a glass diffusion bottle and ~3-4 L min^{-1} clean air was flushed through the diffusion bottle at room temperature and into the chamber to transport H_2O_2 vapor into the chamber. H_2O_2 addition took ~3 hours with this approach. No ozone was added to the chamber. While H_2O_2 was being transported to the chamber, 1 µL deuterated butanol (1-butan-d9-ol, hereafter referred to as butanol-d9) was injected into a clean air stream flowing into the chamber with a syringe and a Swagelok tee and septum. Plant volatiles were thermally desorbed from the adsorbent cartridge samples collected from the plant enclosures previously (see Section 2.1). To accomplish this, a stainless steel manifold was constructed to hold four adsorbent cartridges at one time inside an old GC oven with ¼" PFA tubing running from the end of the cartridges to the environmental chamber. Cartridges were initially flushed with pure nitrogen at room temperature for 5 minutes to remove any residual O_2 before ramping up the GC oven to 200 °C. The GC oven was held at 200 °C for 10 minutes to thermally desorb plant volatiles into the environmental chamber. To standardize the experimental approach and ensure comparability between the different experiments, we aimed to add ~20 ppb monoterpenes in the chamber before initiating oxidation. This ensured at least one class of VOCs remained at a similar mixing ratio across experiments even as other VOC classes potentially changed in response to the aphid stress. This approach allowed us to normalize the experiments by the monoterpene mixing ratio and investigate how relative amounts of other VOC classes influenced SOA yield. To reach this mixing ratio, we desorbed either 4 or 8 adsorbent cartridge samples collected from the plant enclosures for each SOA experiment. Note, this means some experiments were conducted with the cartridges collected from just two of the plants (4 cartridges included the front and breakthrough cartridge from two plants) or all four of the plants. Thus, there would be some variability in the initial VOC profile. Total monoterpene mixing ratio was monitored using the PTR-ToF-MS to evaluate whether or not we needed to desorb additional cartridge samples after the first four cartridges had been desorbed. VOCs were introduced to the chamber using this approach to attain the mixing ratios necessary to conduct the experiments, but it is possible that some VOCs were lost to the lines between the GC oven and the chamber. The limitation of this is we cannot be confident the initial VOC profiles in the

chamber are exactly the same as the VOC emission profiles (for example, if sesquiterpenes were preferentially lost to the lines). However, the goal of this experiment was to investigate oxidation chemistry and SOA production from complex mixtures of biogenic VOCs, and to compare that chemistry between different mixtures collected from a healthy plant and an aphid-stressed plant. While we cannot be sure the mixtures exactly match the emission profile, we very clearly saw a difference between the control (healthy plants) and treatment (aphid-stressed plants) profiles, and consequently were able to probe changes to the resulting chemistry based on the types of emissions that had been induced by the aphid stress treatment.

After adding the plant volatiles to the environmental chamber, we characterized the specific VOC profile (e.g. types and quantity of individual compounds in the chamber) at the beginning of each chamber experiment. To accomplish this, we sampled from the chamber onto a clean pair of adsorbent cartridges by pulling 0.4-0.5 L min^{-1} chamber air through two sampling cartridges for 20 minutes. These were analyzed off-line to provide us with quantitative, detailed chemical speciation of the plant volatiles in the environmental chamber at the beginning of each experiment. The final step before starting the experiment was to use a TSI constant output atomizer to add polydisperse dried ammonium sulfate seed particles (~5,000 p/cc in the chamber). Photooxidation was initiated by turning on the 340 nm LED lamps installed along the side of the chamber. After oxidation was initiated, all incoming flows to the environmental chamber were shut off and the chamber was operated in batch mode. Oxidation of VOCs and SOA production and growth were monitored for a minimum of 7 hours.

The approach used for dark ozonolysis experiments was similar to the methods described in the previous paragraph with the following exceptions: no H_2O_2 or d9-butanol was added to the chamber and the lights were kept off. Instead, oxidation was initiated by adding a 50-second pulse of ozone from a custom-built ozone generator that corresponded to an initial ozone mixing ratio in the chamber of 50 ppb in the absence of VOCs. This initial ozone mixing ratio value was characterized in the absence of VOCs because many of these plant volatiles are highly reactive with ozone, and thus began reacting ozone away immediately upon ozone introduction to the chamber. No OH scavenger was added to the chamber so these experiments should be thought of as "ozone-initiated" because ozonolysis produces HOx radicals that can participate in oxidation chemistry[42].

For comparison with previously published SOA chamber results, experiments were performed using an α-pinene VOC standard for both dark ozonolysis and photooxidation experiments. For the α-pinene experiments, 0.8 µL of 99% purity α-pinene standard was injected into a clean air stream flowing into the chamber with a syringe and a Swagelok tee and septum. No cartridge samples were collected from the chamber before initiating oxidation in α-pinene experiments. In this case, the PTR-ToF-MS was sufficient to monitor VOC mixing ratios because no other monoterpene isomers were present in the chamber.

2.3. *Instrumentation*

Gas-phase volatiles and oxidation products were monitored continuously with a PTR-ToF-MS (PTR 8000; Ionicon, Inc.) and acetate-CIMS (Aerodyne, Inc.). The PTR-ToF-MS sampling line was composed of ~7 m ¼" PFA tubing heated to a temperature of 50 °C and insulated with a flow rate of ~5 L min^{-1}. The PTR pulled from this sampling flow with 1 m PEEK tubing (1 mm i.d.) heated to a temperature of 60 °C at a flow rate of .200 L min^{-1}. The PTR-ToF-MS design and working principle has been described in detail in several previous publications[43–46]. In this study, the PTR-ToF-MS was operated under the following conditions: 2.3 mbar drift tube pressure, 600 V drift tube voltage, 130 Td E/N, and 60 °C temperature of the drift tube. PTR-ToF-MS data were pre-processed (including mass scale calibration and peak fitting) by PTR-MS Viewer software v.3.2 (Ionicon Analytik GmbH), and further analyzed by Igor Pro v.6.37 (Wavemetrics, Inc.). After data pre-processing the background noise of the instrument was subtracted from the signals, before further data analysis. Moreover, the PTR-ToF-MS signal intensities were corrected for the transmission efficiency of ions with different molar masses using a calibration gas standard containing 8 aromatic compounds with mixing ratios ~100 ppbV in nitrogen (BOC, United Kingdom). In addition to this, we have corrected the monoterpene signal for known fragmentation patterns of the most abundant monoterpenes measured with the GC during each experiment (i.e. a-pinene, 3-carene, limonene) using the ion product distributions characterized for this instrument and published previously in Kari et al.[47]. The final (reported) monoterpene concentration was calculated accounting for monoterpene fragmentation as described in Kari et al.[48] (Appendix 2).

An Aerodyne time-of-flight chemical ionization mass spectrometer (ToF-CIMS) was used to measure VOC oxidation products with acetate ionization, a chemical ionization technique

sensitive to acidic compounds. The ToF mass spectrometer of the instrument is described in detail elsewhere[49], and the acetate ionization scheme is discussed and characterized in various previous studies[50–52]. The ToF-CIMS sampling line was 2 m 3/8" PFA tubing that pulled 2 L min^{-1} from the same sampling line that served the PTR, but the ToF-CIMS line was upstream of the PTR instrument (directly adjacent to the chamber). This comparatively short inlet line was designed to minimize vapor wall interactions in the lines, and was achieved by keeping the acetate-CIMS instrument inside the chamber room directly adjacent to the chamber itself. Upon entering the instrument, gas-phase compounds were subject to ionization at 100 mbar in the ion-molecule reaction (IMR) region. Ions are subsequently guided through several differentially pumped chambers containing ion-guidance elements to the ToF mass spectrometer (10^{-6} mbar). For creating the acetate reagent anions, a flow of 0.050 L min^{-1} of N_2 was first passed through the headspace of an acetate anhydride reservoir and then diluted into a 2 L min^{-1} N_2 carrier flow. The flow passed over a ^{210}Po alpha source (P-2021, NRD) prior to entering the IMR. In the common reaction pathway in the IMR that ionizes sample molecules, an acetate anion will abstract a proton from a sample molecule if the sample molecule possesses a higher gas phase acidity than that of acetic acid. Alternatively, acetate anions may also form adducts with sample molecules. The first chamber after the IMR was pumped to 2 mbar, and the DC voltages on its ion-guidance elements were set to promote collisions of ions with surrounding gas to break clustered adducts. This is common practice in acetate-CIMS and facilitates data analysis[53]. A measure of the efficiency of that adduct declustering is the ratio of the acetate-acetic acid "dimer" ion (m/z 119) to the acetate reagent ion (m/z 59). That ratio was ~2% throughout this study. We therefore assumed that all observed ions were deprotonated compounds, specifically with gas-phase acidities greater than the acidity of acetic acid. However, some may also be fragments produced inadvertently by the collisions in the ion-guidance elements[53]. ToF-CIMS data was processed and analyzed using tofTools[49], a purpose-built data analysis package running on MATLAB (Mathworks Inc). The mass axis calibration of the acetate-CIMS was performed in the tofTools analysis software using known background ion signals during empty chamber periods and background signals plus known oxidation compound signals (such as pinic acid and pinonic acid) during oxidation periods. Used background ions were "HCOO- (formic acid)", "NO3- (nitric acid)" and "CH3COOHCH3COO- (acetic acid cluster)". These mass calibration signals give robust calibration over the mass axis of interest with average mass accuracy of 1-3

ppm." All ToF-CIMS data presented in this paper is based on relative signal; we do not present any absolute mixing ratios of the gas-phase oxidation products. We note that Aljawhary et al.[52] (Fig. 5) have shown acetate-CIMS sensitivities tend to be higher for more volatile compounds. This suggests our volatility basis sets could be biased toward the higher volatility material without having taken this into account.

The initial VOC profiles in the chamber, including speciated terpene structural isomers, were characterized at one sampling time point before the initiation of oxidation chemistry in each plant SOA experiment by collecting samples onto multi-bed adsorbent cartridges and analyzing cartridges off-line with a thermo-desorption gas chromatograph mass spectrometer (TD: Perkin Elmer, ATD 400, USA; GC-MS: Hewlett Packard, GC 6890, MSD 5973, USA). The GC was equipped with a DB-5 column and the following compounds were included in GC standard mixtures: α-pinene, camphene, sabinene, β-pinene, β-myrcene, d-3-carene, limonene, 1,8-cineole, γ-terpinene, terpinolene, linalool, E-4,8-dimethyl-1,3,7-nonatriene (E-DMNT), camphor, borneol, terpinen-4-ol, α-terpineol, bornyl acetate, longifolene, trans-β-farnesene, α-humulene, α-copaene, trans-caryophyllene, aromadendrene, β-elemene, cis-ocimene, allo-ocimene, caryophyllene oxide, cis-3-hexen-1-ol, trans-2-hexenal, 1-hexanol, 1-octen-3-ol, cis-3-hexenyl acetate, nonanal, cis-3-hexenyl butyrate, methyl salicylate, cis-3-hexenyl isovalerate, and cis-3-hexenyl tiglate. We did not have individual GC standards for all of the compounds measured in the chamber because many of these plant volatile compounds do not have commercial standards readily available for purchase. In our case, these compounds cannot be ignored simply because we don't have a standard when our goal is to probe the oxidation chemistry of a complex mixture of plant volatiles. This is because the compounds are present, and could be contributing to SOA production. Compounds without a matching standard will be marked with an asterisk in subsequent figures, and should be considered semi-quantitative. All semi-quantitative compounds were identified using the NIST database with >85% match.

Particle size distributions and particle composition were monitored with a scanning mobility particle sizer (SMPS: TSI, Inc. model DMA 3082, CPC 3775) and a high resolution time-of-flight aerosol mass spectrometer[54,55] (HR-ToF-AMS: Aerodyne, Inc.), respectively. The HR-ToF-AMS was calibrated with monodisperse ammonium nitrate particles. All particle sampling lines were composed of copper or stainless steel tubing.

2.4.   Calculations

Particle wall loss in the chamber was characterized by injecting polydisperse dried ammonium sulfate aerosol into the environmental chamber and monitoring particle wall loss with the SMPS. The size-dependent wall loss coefficient, β (s^{-1}), was calculated for each particle size bin and fit to a polynomial similar to methods described in VanReken et al.[56]. This polynomial was used to calculate cumulative particle mass lost to the walls in each size bin at each time point. The particle wall loss curve and an example of a time-series with wall loss corrected particle mass is shown in the supplemental information (Figure S1 and S2). Recent studies have demonstrated that vapor deposition to chamber surfaces can be substantial[57–68]. However, the vapor wall loss rates can vary depending on volatility and reaction kinetics of the SOA precursors, and no data exists to estimate vapor wall losses from the complex mixture of VOCs used in these chamber experiments. Consequently, the SOA yields reported here have not accounted for vapor deposition and could be considered a lower bound.

In photooxidation experiments, OH exposure was estimated from the decay of butanol-d9 following the methods described in Barmet et al.[69]. Briefly, OH concentration was estimated by plotting the natural log of butanol-d9 concentration over time. The slope of the butanol decay curve is related to OH concentration with the following equation:

$$m= -k_{butanol-d9} * [OH] \qquad \text{(Eq. 1)}$$

where m is the slope of the butanol decay curve and k is the reaction rate constant between butanol-d9 and OH (k=3.4×10^{-12} molecules cm^{-3} s^{-1}). Based on the slopes of the butanol decay in each experiment, the average OH concentration in the chamber experiments ranged from 2.1-2.9×10^{6} molecules cm^{-3}. The OH exposure was calculated from the OH concentration by integrating the concentration over the length of the experiment (units: molecules cm^{-3} s). OH exposures in the chamber experiments in this study ranged from 5.5-9.5×10^{10} molecules cm^{-3} s with a corresponding photochemical age of 10.2-17.5 hours, assuming atmospheric OH concentration equal to 1.5×10^{6} molecules cm^{-3}.

Saturation concentrations (C_{sat}) at 298 K of oxidized organics were estimated based on the number of carbon and oxygen atoms in each molecule according to the parameterization by Li et al.[70] The compounds were then grouped based on their C_{sat} in volatility bins between 10^{-10} and 10^{9} $\mu g/m^3$, where the limits for a bin 10^{x} $\mu g/m^3$ were $10^{x-0.5}$-$10^{x+0.5}$ $\mu g/m^3$. The VBS for the gas phase compounds was presented based on summed mass fractions of compounds in each

volatility bin. Compounds of lower C_{sat} than the considered volatility range were counted in the lowest volatility bin, respectively.

SOA mass yields were calculated as the mass of condensed organic aerosol formed divided by the mass of reacted VOCs that were observed in the chamber. The mass of condensed organic aerosol generated in each experiment was estimated from SMPS data and corrected for particle wall losses. The potential range of SOA mass yields was calculated assuming SOA density of 1.0-1.5 g cm^{-3}, which is consistent with a reasonable range for SOA generated from Scots pine emissions[17]. The initial SOA precursors identified in the chamber in each experiment included monoterpenes, sesquiterpenes, and aromatics (based on PTR-ToF-MS and TD-GC-MS data). The amount of VOCs that reacted in the chamber was calculated from a combination of GC and PTR data. Reacted monoterpenes and aromatics were measured continuously using the PTR-ToF-MS data. In the ozone experiments, 50-80% of the initial monoterpenes had reacted away by the end of the experiment with the range representing variation between the three ozonolysis experiments. In the OH experiments, >90% of monoterpenes had reacted away by the end of the experiment. An example time-series illustrating reaction of monoterpenes during an ozone experiment and an OH experiment is shown in the supplementary information (Figure S3). Thus, the ozonolysis experiments were more oxidant-limited systems than the OH experiments. The aromatic compounds did not react in the ozonolysis experiments and were less reactive with OH than the monoterpenes, with 65-70% of p-cymene reacting, 17-44% of phenol reacting, and 13-36% of methyl salicylate reacting. Unfortunately, we observed substantial PTR under-prediction of sesquiterpenes based on a GC/PTR inter-comparison, and thus concluded the PTR sampling lines were too long to directly measure sesquiterpene mixing ratios with the PTR. However, given the highly reactive nature of sesquiterpenes with ozone and OH, we assumed all sesquiterpenes reacted in all the experiments. Therefore the mass of reacted VOC was as the sum of the observed change of monoterpene concentration, observed change of aromatics concentration and estimated change of sesquiterpene concentration calculated from the initial concentration and assumed final concentration of zero. All known major SOA-forming precursors would be detected with the combined PTR and TD-GC-MS data. Due to the complex nature of the plant volatile mixture, it is possible we have under-predicted the amount of reacted VOCs if some potential SOA-forming precursors were missed. In light of this, the SOA mass yields presented here should be considered upper limits.

3. RESULTS AND DISCUSSION

3.1. *Overview of Chamber Experiment Conditions*

A summary of the VOC emission profiles in the chamber at the start of the experiment is shown in Figure 2. These values reflect the average initial VOC profile for all healthy Scots pine experiments (N=3) and all aphid-stressed Scots pine experiments (N=3). Monoterpene mixing ratios did not significantly differ between the two types of experiments with 18.1 ppb and 19.2 ppb for healthy and aphid-stressed experiments, respectively (p-value=0.6). Recall, the experimental design targeted adding ~20 ppb monoterpenes to the chamber for each experiment to ensure comparability, and thus these results confirm that, on average, that target was accomplished. Other compound classes identified in the cartridge samples, and shown in the figure, include sesquiterpenes and aromatics. Methyl salicylate (MeSA) is an aromatic plant hormone, but has been presented separately from other aromatics because it has been implicated in plant stress response to aphids[18]. Other aromatic compounds included phenol, 2-allyltoluene, phenethyl alcohol, and the cymene isomers. Initial mixing ratios of other aromatic compounds was similar in both sets of experiments with 3.7 ppb and 4.0 ppb in healthy and aphid-stressed experiments, respectively (p=0.9).

The largest difference in potential SOA precursors between healthy and aphid-stressed experiments was observed in sesquiterpene mixing ratios. In the healthy pine SOA experiments, initial sesquiterpene mixing ratios were 1.4 ppb. In the aphid-stressed SOA experiments, initial sesquiterpene mixing ratios were 7.9 ppb. This is a marginally statistically significant difference (p<0.01) and the results agree with other observations of induction of sesquiterpene emissions from trees by aphid feeding[18,71]. Furthermore, aphids are capable of emitting small amounts of the sesquiterpene, *E*-β-farnesene, when disturbed[72]. We did not observe a difference in average methyl salicylate mixing ratios in the chamber between healthy (1.2 ppb) and aphid-stressed (0.87 ppb) experiments, in contrast with other aphid-plant stress emission studies[18,73]. The overall contribution of methyl salicylate to total emissions was low in both types of experiments. It is possible the methyl salicylate stress effect was smaller in our study because we collected emissions from the "whole-plant" level in contrast to other plant stress emission studies, which have found elevated methyl salicylate emissions at the site of aphid damage[18,73]. An alternative explanation could be related to the cool laboratory temperature. Methyl salicylate has been linked to aphid herbivory in conifers in conjunction with heat stress[74,75], which is a typical

condition during natural aphid outbreaks. In our case, the plants were brought into the cool laboratory so this could have altered aphid feeding behavior and reduced methyl salicylate emissions from the stressed plants. Finally, despite our best efforts to keep the healthy plants as "healthy" as possible, we did notice some fungal growth in the enclosures of the healthy plants. Prior to being used for the experiments, these plants were watched carefully and any aphids, or other insects, were removed as quickly as possible during shoot growth in late Spring. However, there may have been some residual insect feces or aphid honeydew on the plants that fostered a good environment for fungal growth, particularly when the plant was placed in a humid environment in the enclosure. Fungi that emit methyl salicylate have been shown to grow on insect feces or honeydew[76–78], so this could have been another reason we did not observe a difference between the healthy control and aphid-stressed methyl salicylate mixing ratios in the chamber. However, even though we did not observe an expected elevation of methyl salicylate in the chamber during the aphid-stressed experiments, there were clear differences in sesquiterpene emissions that would be relevant for SOA formation.
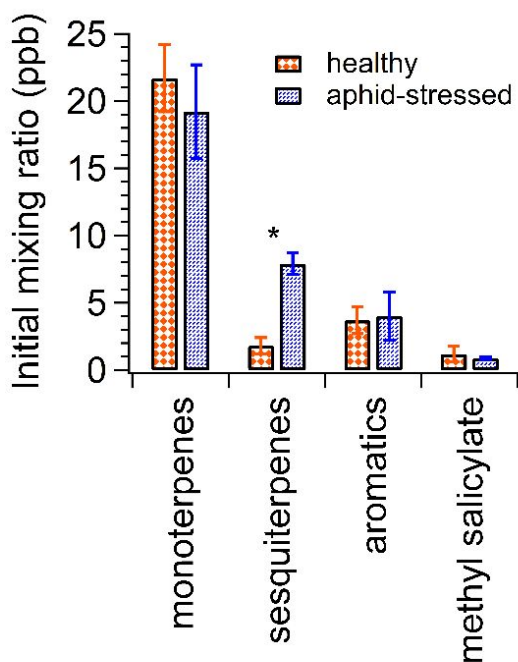

Figure 2: Average VOC mixing ratio in the chamber at the start of the experiment for healthy (N=3) and aphid-stressed (N=3) experiments. Asterisk indicates statistical significance (p<0.001) with a Student's t-test. Error bars are standard error of the mean.

A summary of all SOA chamber experiments, and relevant information for each, is given in Table 1. Each experiment was provided with a unique experimental ID for reference throughout the text. The table shows the initial chamber concentrations for total monoterpenes, sesquiterpenes, aromatics, and methyl salicylate before oxidation was initiated. These values were calculated from the cartridge samples collected from the chamber before each experiment and analyzed off-line with the TD-GC-MS.

Three dark ozonolysis chamber experiments were conducted: one using aphid-Stressed Scots pine emissions (S-O3), one using Healthy Scots pine emissions (H-O3), and one with a well-studied monoterpene standard, α-pinene, to place our results in context with other SOA chamber experiments (AP-O3: "AP"=α-pinene). The SOA yield shown in Table 1 from oxidation of aphid-stressed VOCs was similar to the yield from α-pinene with SOA mass yields of 6.9-10.4% (S-O3) and 6.3-9.4% (AP-O3). However, making direct comparisons between SOA mass yields from experiment to experiment is made more complicated by differences in the mass of total reacted VOCs and total condensed organic aerosol mass. Absorption-partitioning theory states that the SOA mass yield for any given SOA precursor increases at increasing condensed organic aerosol mass[79,80]. Thus, it is important to consider that the total reacted VOCs and condensed organic aerosol mass (which was equivalent to the SOA mass formed in these experiments) was higher in the aphid-stressed experiment (S-O3) than AP-O3, and thus the aphid-stressed SOA mass yield was comparably lower than that for α-pinene after accounting for absorption effects. The α-pinene SOA mass yield in experiment AP-O3 was consistent with the 3.2-10% yield presented previously for α-pinene ozonolysis at similar organic aerosol mass loadings[81]. The healthy experiment, H-O3, had a higher SOA yield in comparison to the other two ozonolysis experiments, even after accounting for absorption effects. Notably, the SOA yield was higher in the healthy plant experiment despite the initial sesquiterpene mixing ratio being much lower than the aphid-stressed experiment. This result was surprising given the ample evidence showing that sesquiterpenes have very high SOA mass yields[82–85], and that sesquiterpenes can substantially increase SOA yields from a complex mixture of plant volatiles even when they contribute just 10-30% of the total VOC profile[17]. Potential mechanisms for this unexpected sesquiterpene depression of SOA yields will be discussed in more detail in the next section (section 3.2: Ozonolysis Chemistry).

Table 1: Summary of SOA chamber experiments and relevant information.

Oxidant	VOC Source	Exp ID	MT_i[a]	SQT_i[a]	Aro_i[a]	$MeSA_i$[a]	ΔVOC[b]	ΔSOA[c]	SOA yield[d] (%)
O₃	aphid stressed	S-O3	120.4	72.8	40.2	6.1	157.7	10.9-16.4	6.9-10.4
	healthy	H-O3	148.9	5.9	20.6	1.4	82.3	8.0-12.0	9.7-14.6
	α-pinene	AP-O3	94.8	-	-	-	74.8	4.7-7.0	6.3-9.4
OH	aphid stressed	S-OH-1	68.6	52.7	9.0	4.2	125.6	22.2-33.3	17.8-26.6
	aphid stressed	S-OH-2	131.6	73.6	11.1	5.9	207.2	36.4-54.6	17.9-26.8
	healthy	H-OH-1	101.5	25.1	20.4	14.5	138.7	14.7-22.0	10.8-16.3
	healthy	H-OH-2	112.6	15.1	7.9	7.1	129.2	19.9-29.9	15.5-23.2
	α-pinene	AP-OH	45.2	-	-	-	43.4	2.6-3.9	6.0-9.1

[a]*MTi, SQTi, Aroi, and MeSAi refer to the initial concentration measured in the chamber before oxidation was initiated.*

[b]*Reacted VOCs were estimated as described in the text.*

[c]*The SOA formed in the chamber is estimated from SMPS data and corrected for particle wall losses, and the range is provided for SOA density from 1.0-1.5 g cm⁻³. That range is reflected in the SOA yield also.*

[d] *SOA yield was calculated as $\frac{\Delta SOA}{\Delta VOC}$*

All units are µg m⁻³ except where indicated otherwise.

Five photooxidation experiments were conducted: two using aphid-stressed Scots pine emissions (S-OH-1 and S-OH-2), two using healthy Scots pine emissions (H-OH-1 and H-OH-2), and one α-pinene (AP-OH). In general, SOA mass yields from photooxidation experiments was higher than for ozonolysis experiments. S-OH-1 and H-OH-2 had approximately the same mass of reacted VOCs and also had very similar SOA mass yields of 17.8-26.6% and 15.5-23.2% for aphid-stressed (S-OH-1) and healthy (H-OH-2), respectively. Experiment S-OH-2 had

substantially higher reacted VOCs, but a similar SOA mass yield of 17.9-26.8%. H-OH-1 had slightly higher reacted VOCs and lower SOA mass yields than the other three OH experiments with an estimated SOA mass yield of 10.8-16.3%. After considering absorption effects, the SOA formation potential of the VOC profiles in S-OH-2 and H-OH-1 were lower than their paired "healthy" or "aphid-stressed" experiment. Similar to the ozonolysis experiments, the initial sesquiterpene concentration was higher in both aphid-stressed experiments than the healthy experiments. Unlike the ozonolysis experiments, the photooxidation experiments did not exhibit a clear sesquiterpene depression in SOA yields. Potential explanations for this will be discussed in section 3.3 on Photooxidation Chemistry. The α-pinene photooxidation experiment, AP-OH, had a SOA mass yield of 6.0-9.1%, which is low compared to other reports. For example, with 109 µg m^{-3} reacted α-pinene, Eddingsaas and colleagues reported an SOA mass yield of 36.7%[86]. First-generation oxidation products of α-pinene can continue to react and contribute to SOA production. For example, myrtenal is an α-pinene oxidation product that, upon further oxidation, can contribute up to 23% of total α-pinene SOA[37]. The low α-pinene yield reported for AP-OH indicates that the photooxidation experiments in this study may have also been oxidant limited, and there was not enough OH to continue oxidizing subsequent reaction products. However, α-pinene photooxidation experiments conducted in the SAPHIR chamber reported 2.1-5% SOA mass yield under similar OH exposures to the experiments reported here (Zhang et al., 2015, 2018). These SOA mass yields are consistent with the values we observed[87,88].

A summary of the elemental analysis of particle organic composition is shown in a Van Krevelen diagram (Figure 3). The oxygen-to-carbon (O:C) and hydrogen-to-carbon (H:C) ratios were estimated from the HR-ToF-AMS data using the algorithm presented previously[89]. Ozonolysis experiments are shown in triangles and photooxidation experiments in squares with each individual experiment shown in a different color. The α-pinene experiments are shown in black. Some of the major gas-phase volatiles in the chamber at the start of the experiments are noted and labeled. All the ozonolysis experiments cluster together with an H:C just under 1.5 and an O:C around 0.60-0.65. The healthy and aphid-stressed photooxidation experiments clustered together with an H:C around 1.6 and an O:C around 0.65-0.70. The α-pinene photooxidation experiment had the lowest O:C of all experiments at 0.45-0.50. All experiments fall within the "ambient zone" on the Van Krevelen diagram as defined from the dashed lines described further in Ng et al.[90].
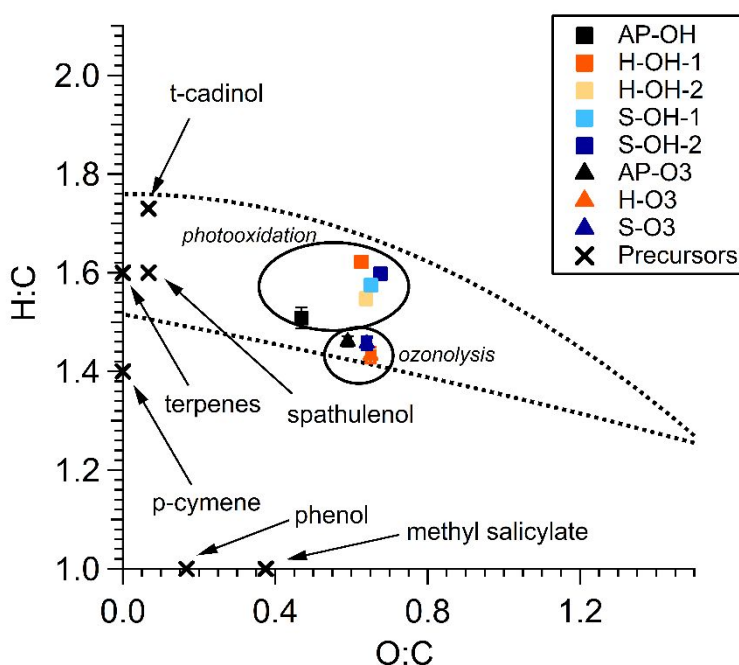
Figure 3: Van Krevelen diagram summarizing elemental analysis of SOA from all experiments. Dashed lines indicate the typical "ambient zone" described in Ng et al., (2010). The major gas-phase precursors identified from the GC data are shown with text labels. Photooxidation and ozonolysis experiments are encircled separately and labeled.

3.2.   *Ozonolysis chemistry*

To understand the gas-phase oxidation chemistry and SOA formation chemistry in any individual chamber experiment, it is informative to look at the VOC profile for each individual experiment. For that reason, the VOC profiles for monoterpenes and sesquiterpenes are shown in Figure 4 for the individual dark ozonolysis experiments. Aromatic compounds (including methyl salicylate) were excluded because they would not react readily with ozone and consequently would not be major contributors to the oxidation chemistry in these experiments. Recall, we did not have individual GC standards for all of the compounds shown because many of these compounds do not have commercial standards available for purchase. Those compounds are marked with an asterisk and should be considered semi-quantitative. A complete list of the standards and the approach used to identify and quantitate compounds without standards is provided in the Methods section (Section 2.3: Instrumentation). The seven dominant monoterpenes identified in the experiments were α-pinene, 3-carene, limonene, camphene, β-

phellandrene, myrcene, and β-pinene. The "other" monoterpenes category includes tricyclene, β-fenchene, α-fenchene, verbenene, α-phellandrene, α-terpinene, sabinene, 1,8-cineole, β-ocimene, γ-terpinene, and camphor. The large error bar for "other" monoterpenes in the healthy ozonolysis
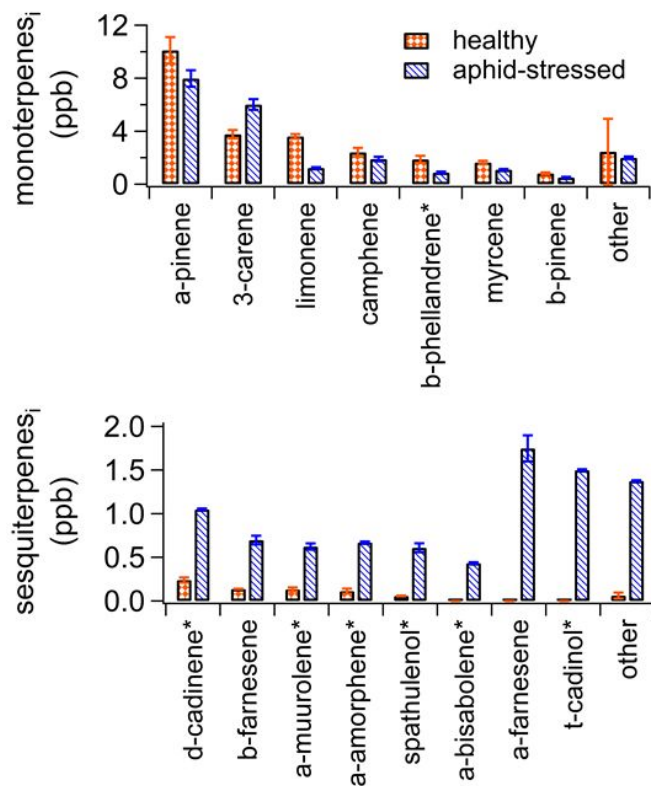

Figure 4: The initial VOC profiles before ozone was added to the chamber for the healthy (H-O3) and aphid-stressed (S-O3) experiments. Error bars denote the standard deviation of duplicate cartridge samples. Standard deviation was propagated for the "other" category by taking the square root of the sum of squares of individual standard deviations for each compound. An asterisk (*) denotes compounds for which a proxy standard was used.

experiment was driven by large differences between duplicate cartridges for two compounds - tricyclene and β-pinene. Generally, the monoterpene profile looked similar between the two experiments. 3-Carene was slightly higher in the aphid-stressed experiment and limonene was slightly higher in the healthy experiment. Both of these differences would be expected to increase SOA yields in the healthy experiment because 3-carene has relatively low yields and limonene has particularly high yields. However, these small differences between monoterpenes are dwarfed by the large difference in sesquiterpenes.

The eight dominant sesquiterpenes identified in the experiments were δ-cadinene, β-farnesene, α-muurolene, α-amorphene, spathulenol, α-bisabolene, α-farnesene, and t-cadinol. Two of these compounds are sesquiterpene alcohols—spathulenol and t-cadinol. The "other" sesquiterpenes category includes longifolene, β-caryophyllene, 2-Isopropyl-5-methyl-9-methylenebicyclo[4.4.0]dec-1-ene (hereafter referred to as SQT1), β-selinene, γ-muurolene, α-calcorene, and calamenene. The mixing ratio of each of these sesquiterpenes was higher in the aphid-stressed experiment with particularly large increases in α-farnesene, and t-cadinol.
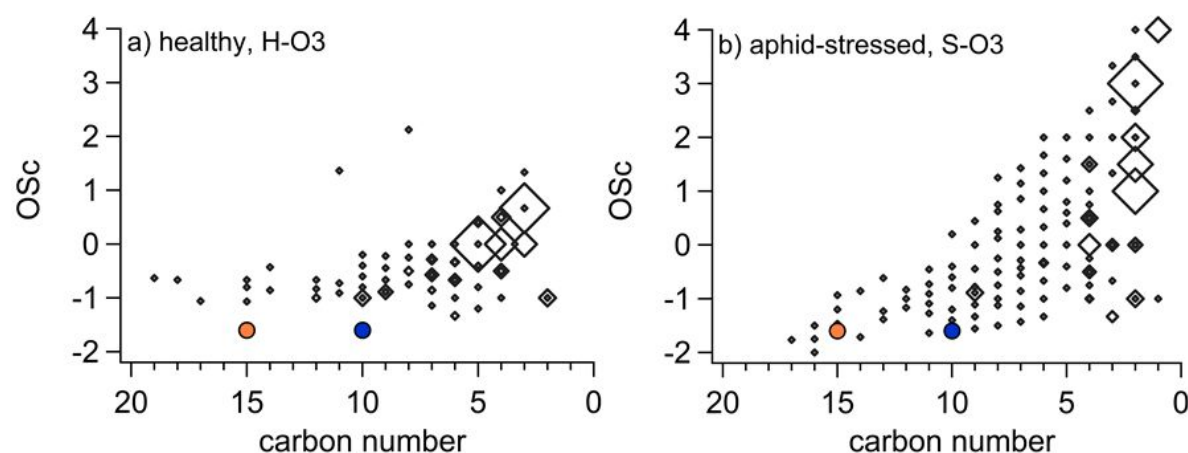

Figure 5: Ozonolysis oxidation products measured in the chamber during the last 30 minutes of the experiment plotted on a 2-D axis of oxidation state (OSc) and carbon number for the a) healthy plant emissions and b) aphid-stressed emissions. Each diamond marker denotes one peak identified in the acetate-CIMS, , and the size of the marker indicates intensity of the signal. Filled circles indicate the location of dominant SOA precursor species in the ozonolysis experiments with (●) for sesquiterpenes and (●) for monoterpenes.

A comparison of all oxidation products measured with the acetate-CIMS during the last thirty minutes of each experiment is shown in Figure 5. Note, acetate-CIMS data from the α-pinene experiment did not pass quality control checks and could not be used for subsequent analysis. Oxidation products were plotted on a two-dimensional axis of oxidation state (OSc) and carbon number. OSc was calculated as OSc=2*O/C-H/C where O/C is the oxygen-to-carbon ratio and H/C is the hydrogen-to-carbon ratio following the methods described by Kroll and colleagues[91]. These plots provide information about the dominant chemical processes occurring in the chamber where the presence of more compounds at higher carbon number and unchanging OSc indicates oligomerization, more compounds at higher OSc and unchanging carbon number indicates functionalization, and more compounds at lower carbon number and higher OSc

indicates fragmentation[91]. The distribution of oxidation products in the aphid-stressed ozonolysis experiments were shifted toward lower carbon number and higher OSc compared to the healthy experiment. This could suggest a higher degree of fragmentation reactions are occurring from the oxidation of VOCs in the aphid-stressed experiment versus the healthy experiment.

To further probe potential mechanisms that could explain an increase in fragmentation reactions during the aphid-stressed experiment, a profile of the different sesquiterpene structures is shown in Figure 6 along with some example chemical structures. Recall, the total
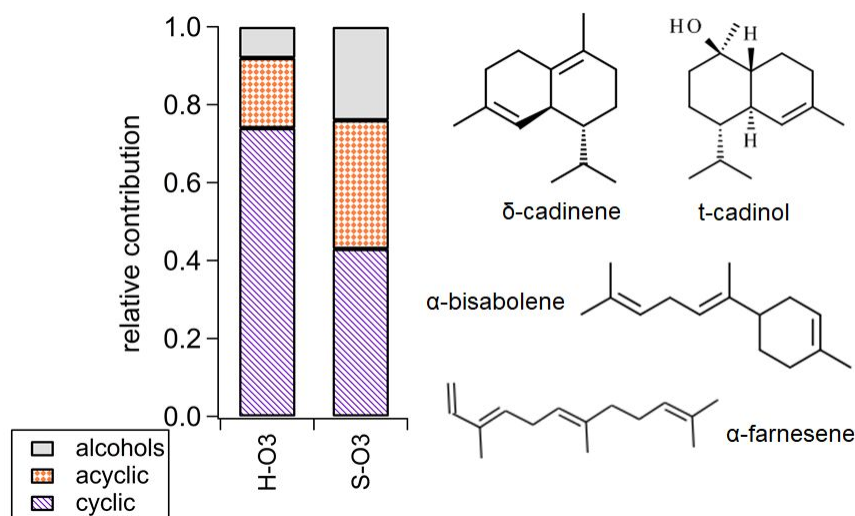

Figure 6: Relative contribution of sesquiterpene classes/structures in the ozonolysis experiments with sample structures of some representative compounds.

sesquiterpene mixing ratios were higher in the aphid-stressed experiment (S-O3), but 1/3 of those sesquiterpenes had an acyclic molecular structure. The dominant sesquiterpenes with acyclic structure or large acyclic chains in the structure include the farnesene isomers and α-bisabolene. When cyclic structures with double bonds located within the ring undergo ozonolysis chemistry, the ring is broken but the number of carbons in the molecule remains unchanged (functionalization reactions). However, when ozone adds across an acyclic double bond, and breaks the bond, the molecule is fragmented into smaller compounds. This is consistent with the trend noticed in the oxidation products shown in Figure 5 and, taken together, suggests increases in acyclic sesquiterpenes lead to increased fragmentation during ozonolysis and reduced SOA mass yields. It is also notable that sesquiterpene alcohols contributed to 23% of the total sesquiterpenes in the aphid-stressed experiment, which contain fewer double bonds, and are thus

less reactive with ozone. These results could also contribute to the reduced SOA mass yields observed for the aphid-stressed experiment in comparison to the healthy and α-pinene experiment.
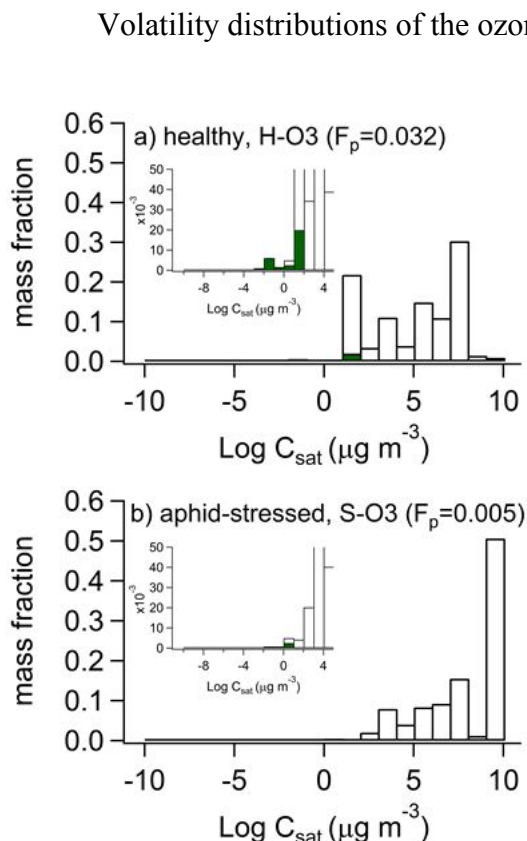
Volatility distributions of the ozonolysis oxidation products measured in the gas-phase with the acetate-CIMS are summarized in Figure 7 with the mass fraction of the total contribution plotted versus the saturation vapor pressure. To compare the "SOA formation potential" of the measured gas-phase oxidation products between experiments, the fraction of each bin expected to undergo gas-particle partitioning ($F_{gp,,i}$) is shown in solid green and calculated with the following equation based on Donahue et al.[92]

$$F_{gp,i} = 1/(1+(C_{sat,i}/C_{oa})) \qquad (Eq. 2)$$

where $C_{sat,i}$ is the saturation vapor pressure of the ith bin and C_{oa} was set to 1 ug m^{-3} as a reasonable approximation for background organic aerosol in a boreal forest[93]. This value was multiplied by the measured gas-phase mass fraction in that bin (M_i). Then, the value was summed across the volatility distribution, and was calculated as

$$F_p = \Sigma M_i * F_{p,i} \qquad (Eq. 3)$$

Chhabra et al.[94] performed similar calculations from acetate-CIMS data with one important difference; their inlet line was heated so the measurements included organics residing in both gas and particle phases. For the data presented here, it is important to emphasize that the shaded area does not indicate the amount of mass predicted in the particles; we did not have a direct measurement of particle composition and the units presented are mass fraction rather than an absolute mass. Rather, the shaded area is intended to provide a metric for comparing the "SOA formation potential" of the measured gas-phase products between experiments. With noted limitations, this value does provide one metric for comparing the potential of the measured gas-

Figure 7: Volatility distributions of the ozonolysis oxidation products measured with acetate-CIMS for the a) healthy plant emissions and b) aphid-stressed emissions. Shaded areas indicate the fraction of the measured gas-phase that would be expected to exist in the particles for a background organic aerosol mass loading of 1 ug m^{-3}.

phase distribution to undergo gas-particle partitioning. This analysis does not account for any oxidation products that exist solely in the particle phase and were not measured with acetate-CIMS, and it does not account for any oxidation products that would not be detectable with the acetate-CIMS.

The highest SOA formation potential of the gas-phase oxidation products was estimated for the healthy ozonolysis experiment (H-O3) with an F_p of 0.032. In contrast, the mass fraction of oxidation products in the aphid-stressed experiment (S-O3) were weighted toward the highest volatility bin with a corresponding lower SOA formation potential ($F_p= 0.005$). These findings are consistent with the explanation that the healthy VOC profile was dominated by cyclic monoterpenes, which produce highly functionalized oxidation products that are more likely to undergo gas-particle partitioning. In contrast, the VOC profile in the aphid-stressed experiment had a higher contribution from acyclic sesquiterpenes, which fragment upon reaction with ozone and generate higher volatility oxidation products that are less likely to undergo gas-particle partitioning. Another explanation for reduced fraction of low volatility oxidation products in the stressed experiments could be attributed to oxidation product scavenging by highly reactive peroxy radicals formed from the acyclic structures. This mechanism of SOA suppression was recently reported from monoterpene/isoprene mixtures[95], and we did not use an OH scavenger to suppress HOx chemistry.

3.3.   *Photooxidation Chemistry*

The chemical mechanisms controlling SOA mass yield in the photooxidation experiments are more challenging to pinpoint than in the dark ozonolysis experiments because the OH radical is more universally reactive with other compounds. In the ozonolysis experiments, we were able to ignore most of the non-terpene volatiles in the chamber, but recall from Figure 2 that there were aromatic compounds in the plant experiments as well. To demonstrate the increased complexity of plant volatile photooxidation chemistry in comparison with α-pinene chemistry, the PTR mass spectra of a healthy and aphid-stressed experiment and an α-pinene experiment are shown (Figure 8). Spectra at the beginning and end of each experiment are shown to demonstrate which peaks were reacting readily in the chamber. Some of the major peaks are labeled with their associated protonated ion. The left column of Figure 8 shows the PTR spectra of experiments H-OH-1 (a), S-OH-1 (b), and AP-OH (c) near the beginning of each experiment. The spectra are an

average over the first thirty minutes of the experiment after the lights were turned on. Oxidation occurred rapidly after lights were turned on, which explains why some oxidation products are already evident in the spectra. The major peaks in the AP-OH start spectrum are monoterpene peaks ($C_{10}H_{17}^{+}$ and monoterpene fragment $C_6H_9^{+}$) and a few small oxidation products ($C_2H_5O_2^{+}$ and $C_3H_7O^{+}$). Formic acid was a major peak in all OH experiments ($CH_2O_2H^{+}$), and this was also observed with the acetate-CIMS. Both the H-OH-1 and S-OH-1 "start" PTR spectra contain the same peaks as the AP-OH spectra. In addition to the monoterpene peaks, the plant experiments show signals from sesquiterpenes ($C_{15}H_{25}^{+}$), methyl salicylate ($C_8H_9O_3^{+}$), and aromatic terpenoids ($C_{10}H_{15}^{+}$). The H-OH-1 experiment also had an evident oxygenated monoterpenoid
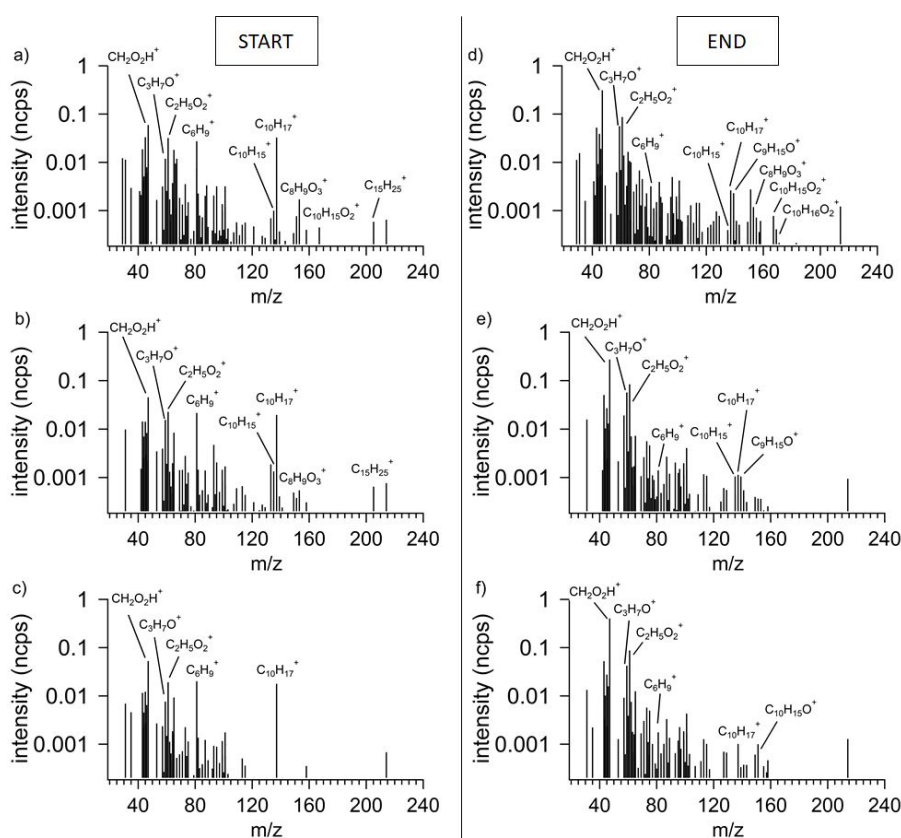

Figure 8: PTR mass spectra at the start (a-c) and end (d-f) of each photooxidation experiment. Representative spectra are shown for H-OH-1 (a and d), S-OH-1 (b and e), and AP-OH (c and f).

signal ($C_{10}H_{15}O_2^{+}$) that was not observed in the S-OH-1 experiment. Thus, comparing the AP-OH starting spectrum with the other two experiments clearly shows the higher molecular complexity in the SOA experiments conducted with plant volatiles as opposed to a single-component standard compound, like α-pinene.

The right column of Figure 8 shows the PTR spectra of H-OH-1 (d), S-OH-1 (e), and AP-OH (f) near the end of the experiment. The spectra were obtained from a 30-minute average approximately 2/3 through the experiment. In AP-OH figure (f), it is evident most of the monoterpenes had reacted (note the log scale on the y-axis) and we could see the generation of monoterpene oxidation products ($C_{10}H_{15}O^+$). All of the sesquiterpenes reacted very rapidly and were no longer present in the "end" spectra in H-OH-1 or S-OH-1. A wide variety of oxidation products with 8+ carbons were observed in both plant experiments as well, but this was particularly true for H-OH-1.

The VOC profiles for the photooxidation chemistry experiments are shown in Figure 9. The seven dominant monoterpenes and the compounds included in the "other" monoterpenes category in the photooxidation experiments were the same as for the ozonolysis experiments described in the previous section. There was no systematic difference in monoterpene profile between the healthy and stressed experiments. Some notable differences were observed in individual experiments. For example, S-OH-1 did not contain any 3-carene, which tends to have lower yields than most monoterpenes, and S-OH-2 had the highest contribution from 3-carene[17]. Recall, some variability in the emission profile could have been introduced based on whether or not cartridges from just two of the trees or all four of the trees were used (see methods for more detail). This could partially explain why the SOA mass yield for S-OH-1 was slightly elevated relative to S-OH-2 after considering expected absorption effects (e.g. S-OH-1 had similar yields as S-OH-2 with a lower total organic aerosol mass loading).

The lower panel of Figure 9 shows the initial mixing ratio of the dominant sesquiterpenes as well as other major contributors like aromatic alcohols (primarily phenol in most experiments) and the aromatic plant hormone, methyl salicylate (MeSA). The aromatic compounds were included in Figure 9 because aromatic compounds are reactive with OH radical. In fact, gas-phase photooxidation chemistry of alkyl benzenoids leads to production of highly oxidized molecules that would be expected to have very high SOA mass yields[96]. Consequently, plant emissions of aromatic compounds would be expected to contribute to SOA formation chemistry in the photooxidation experiments, unlike the ozonolysis experiments. The clearest difference in sequiterpene composition between healthy and stressed experiments was a large increase in acyclic farnesenes in the aphid-stressed experiment. This was also observed in the ozonolysis experiments, and in the previous section we argued this was responsible for the reduction in SOA

mass yields in the aphid-stressed ozonolysis experiments – an acyclic sesquiterpene suppression of SOA production due to increased fragmentation reactions. However, we did not observe a clear "acyclic sesquiterpene suppression" in the photooxidation SOA mass yields (refer to Table 1).
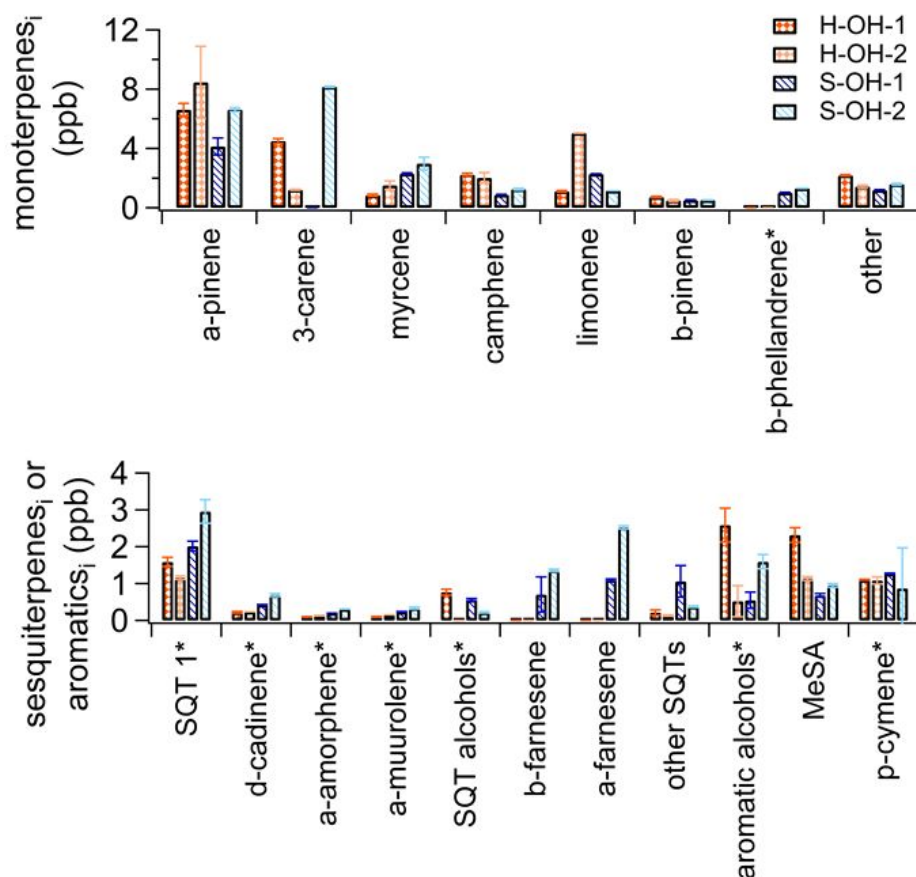

Figure 9: Initial VOC profiles in the chamber for each of the photooxidation experiments before the lights were turned on. Error bars denote the standard deviation of duplicate cartridge measurements. Standard deviation was propagated for the "other" category by taking the square root of the sum of squares of individual standard deviations for each compound. An asterisk (*) denotes compounds for which we did not have a standard and a standard with similar structure was used to quantitate. SQT1= 2-Isopropyl-5-methyl-9-methylenebicyclo[4.4.0]dec-1-ene.

To highlight the influence of sesquiterpenes on photooxidation chemistry, it is useful to start with a comparison of S-OH-1 and H-OH-2; both these experiments had similar total reacted terpenes, and similar SOA mass yields (S-OH-1=17.8-26.6; H-OH-2=15.5-23.2%). H-OH-2 had

a lower mixing ratio of sesquiterpenes in the chamber at the start of the experiment and all those sesquiterpenes had cyclic structures (Figure 10). In contrast, S-OH-1 had a higher mixing ratio of sesquiterpenes in the chamber at the start of the experiment, but only 60% of those sesquiterpenes had cyclic structures. Unlike ozonolysis chemistry which will primarily break double bonds upon reaction, the OH reaction mechanism with farnesene can produce hydroperoxides and functionalize the molecule without breaking the bond[97]. Acyclic sesquiterpenes, such as the farnesenes, had higher SOA mass yields than cyclic sesquiterpenes in a study of OH reaction chemistry of different sesquiterpene structures[98]. In the healthy and aphid-stressed plant photooxidation experiments, we did not see elevated yields from acyclic sesquiterpenes as might be expected based on previous results in the literature for farnesene OH oxidation, but we have already speculated that we had an OH-limited environment and perhaps the yields would have been higher with more oxidant.

   In general, the SOA mass yields were higher from photooxidation than ozonolysis for all experiments. We attribute some of this to the presence of aromatic compounds, such as p-cymene and methyl salicylate, which can produce lower volatility oxidation products that would elevate the SOA mass yields in the photooxidation experiments when compared to the ozonolysis experiments. This is consistent with results showing 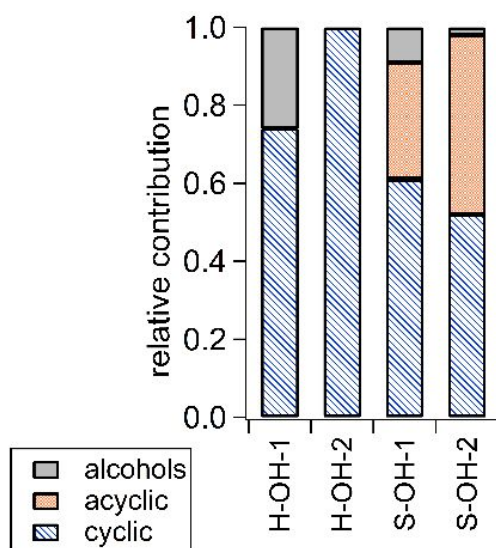elevated SOA mass yields in the presence of methyl salicylate due to plant stress[35]. We note also the large contribution from sesquiterpene alcohols and aromatic alcohols to total initial VOCs. We did not observe a clear relationships between the presence (or absence) of these alcohols and SOA mass yields. However, their abundance in these experiments suggests they should be the topic of future SOA chamber studies.

   If we had reduced fragmentation reactions in the photooxidation experiments, then we might be able to see a smaller mass fraction in the high volatility bins than we observed in the ozonolysis experiments. To investigate this, the volatility distributions of the oxidation products measured with the acetate-CIMS are presented in Figure

Figure 10: Relative contribution from different sesquiterpene structures in the photooxidation experiments

11. The volatility distributions shown were calculated from the average acetate-CIMS spectra measured during the "mid" period of the experiment because the OH experiments exhibited faster chemistry than the ozonolysis experiments (Figure S3). The "mid" period was a 30-minute
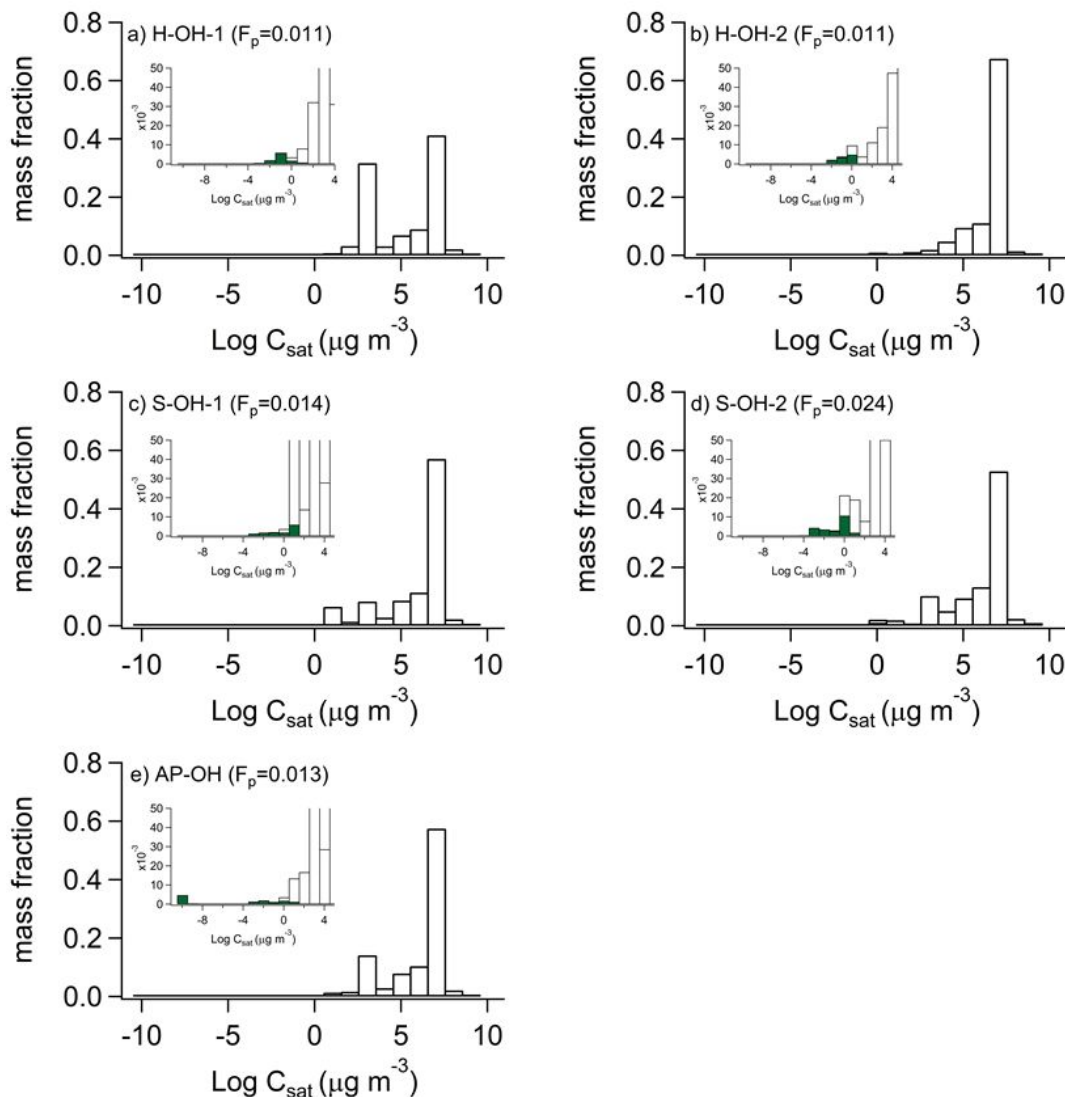

Figure 11:Volatility distributions of the photooxidation products measured with acetate-CIMS for a-b) healthy emissions, c-d) aphid-stressed emissions, and e) α-pinene. Shaded areas indicate the fraction of the measured gas-phase that would be expected to exist in the particles for a background organic aerosol mass loading of 1 ug m^{-3}.

averaging interval that started 3 hours after the experiment start time. It was selected to target a time when oxidation products would be present in the gas-phase and loss of highly oxidized vapors to the chamber wall would be less than at the end. The fraction in the particle phase at

each volatility bin was calculated using the same approach as described in the previous section. Overall, we did not observe a smaller mass fraction of oxidation products in the higher volatility bins for the photooxidation experiments compared to the ozonolysis experiments. Furthermore, we did not see any clear differences between the measured gas-phase volatility distributions of healthy plant oxidation products versus aphid-stress plant oxidation products. This indicates that most of the oxidation products contributing to differences in SOA production are either 1) too low in volatility to be present in substantial amounts in the gas-phase and/or 2) not organic acids and are consequently not detected with an acetate-CIMS.

4. CONCLUSION

This study characterized oxidation products and SOA mass yields from ozonolysis and photooxidation chemistry using the following VOC systems: healthy Scots pine, aphid-stressed Scots pine, and α-pinene. The plant volatile mixtures contained monoterpenes, sesquiterpenes, and various aromatic compounds. The largest difference between the healthy and aphid-stressed volatiles was an increased contribution from sesquiterpenes in the aphid-stressed experiments. In particular, acyclic sesquiterpenes contributed approximately 1/3 of all sesquiterpenes in the aphid-stressed experiments. Sesquiterpene alcohols were also a major contributor to total sesquiterpenes. In the ozonolysis experiments, aromatic compounds were ignored because ozone does not break aromatic rings. Increased acyclic sesquiterpenes led to more fragmentation reactions. This produced higher volatility oxidation products, which decreased SOA mass yield. This result could have broader-scale implications because many plant stress studies have shown increases in acyclic terpene emissions like β-ocimene, β-myrcene, and the farnesenes following a variety of different abiotic and biotic stressors[9,11].

Results from the photooxidation experiments were more difficult to interpret because the OH radical not only reacts with the terpenes, but it also reacts with the aromatic compounds present in the plant volatile profile. SOA mass yields were higher in the plant photooxidation experiments compared to the ozonolysis experiments. We hypothesize two potential mechanisms for this. First, OH radicals can functionalize acyclic sesquiterpenes without breaking the double bond, and consequently we did not observe an "acyclic sesquiterpene SOA suppression" in the photooxidation experiments. Second, the presence of aromatics in the chamber produced lower volatility oxidation products that would have high SOA mass yields. Unfortunately, we did not

directly observe the lower volatility oxidation products that could explain these results with the instrumentation used in this study. However, if plant aromatics do contribute substantially to SOA production, this result could have broader-scale implications because plant emissions of aromatic compounds into the atmosphere are similar to those of all anthropogenic sources combined[99]. These results suggest that those plant aromatic volatiles could be an under-studied source of SOA in the atmosphere.

The results from these experiments have important implications for how increased plant stress in a changing climate could influence SOA production. The biggest difference in the volatile profiles between the healthy and aphid-stressed plants in this study was a clear increase in acyclic sesquiterpenes in the stressed plant experiments. Acyclic sesquiterpenes had very different effects on SOA production depending on the chemical oxidation mechanism. They suppressed SOA formation from ozonolysis, and did not appreciably change SOA production from photooxidation. It is important to consider that OH and ozone are both present in the ambient atmosphere. Acyclic sesquiterpenes, like the farnesenes, have four reactive double bonds and consequently react very rapidly with ozone. In the natural environment, we would expect ozonolysis chemistry would be competitive with OH if atmospheric volatiles had an increase in acyclic sesquiterpenes. Consequently, reduced SOA mass yields could occur in an ambient environment in the presence of ozone. This study clearly highlights the potential importance of acyclic terpene chemistry in a future climate regime with increased presence of plant stress volatiles. Future studies should target these compounds for detailed SOA studies investigating other oxidant regimes, including mixed oxidant systems and in the presence of nitrogen oxides.

5. Acknowledgments

6. Supporting Information

Particle wall loss coefficients as a function of particle diameter (Figure S1), example time-series of particle mass before and after particle wall loss correction (Figure S2), time-series of

monoterpene mixing ratios in the chamber during a sample ozonolysis and photooxidation

experiment (Figure S3)

REFERENCES

(1)   Hallquist, M.; Wenger, J. C.; Baltensperger, U.; Rudich, Y.; Simpson, D.; Claeys, M.; Dommen, J.; Donahue, N. M.; George, C.; Goldstein, A. H.; et al. The Formation, Properties and Impact of Secondary Organic Aerosol: Current and Emerging Issues. *Atmos. Chem. Phys.* **2009**, *9* (14), 5155–5236. https://doi.org/10.5194/acp-9-5155-2009.

(2)   Mahowald, N.; Ward, D. S.; Kloster, S.; Flanner, M. G.; Heald, C. L.; Heavens, N. G.; Hess, P. G.; Lamarque, J.-F.; Chuang, P. Y. Aerosol Impacts on Climate and Biogeochemistry. *Annual Review of Environment and Resources* **2011**, *36* (1), 45–74. https://doi.org/10.1146/annurev-environ-042009-094507.

(3)   Knudsen, J. T.; Eriksson, R.; Gershenzon, J.; Ståhl, B. Diversity and Distribution of Floral Scent. *Bot. Rev* **2006**, *72* (1), 1. https://doi.org/10.1663/0006-8101(2006)72[1:DADOFS]2.0.CO;2.

(4)   Dudareva, N.; Negre, F.; Nagegowda, D. A.; Orlova, I. Plant Volatiles: Recent Advances and Future Perspectives. *Critical Reviews in Plant Sciences* **2006**, *25* (5), 417–440. https://doi.org/10.1080/07352680600899973.

(5)   Sindelarova, K.; Granier, C.; Bouarar, I.; Guenther, A.; Tilmes, S.; Stavrakou, T.; Müller, J.-F.; Kuhn, U.; Stefani, P.; Knorr, W. Global Data Set of Biogenic VOC Emissions Calculated by the MEGAN Model over the Last 30 Years. *Atmospheric Chemistry and Physics* **2014**, *14* (17), 9317–9341. https://doi.org/10.5194/acp-14-9317-2014.

(6)   Carlton, A. G.; Wiedinmyer, C.; Kroll, J. H. A Review of Secondary Organic Aerosol (SOA) Formation from Isoprene. *Atmospheric Chemistry & Physics* **2009**, *9*, 4987–5005. https://doi.org/10.5194/acp-9-4987-2009.

(7)   Barsanti, K. C.; Carlton, A. G.; Chung, S. H. Analyzing Experimental Data and Model Parameters: Implications for Predictions of SOA Using Chemical Transport Models. *Atmospheric Chemistry and Physics* **2013**, *13* (23), 12073–12088. https://doi.org/10.5194/acp-13-12073-2013.

(8)   Niinemets, Ü. Mild versus Severe Stress and BVOCs: Thresholds, Priming and Consequences. *Trends in Plant Science* **2010**, *15* (3), 145–153. https://doi.org/10.1016/j.tplants.2009.11.008.

(9)   Niinemets, Ü. Responses of Forest Trees to Single and Multiple Environmental Stresses from Seedlings to Mature Plants: Past Stress History, Stress Interactions, Tolerance and Acclimation. *Forest Ecology and Management* **2010**, *260* (10), 1623–1639. https://doi.org/10.1016/j.foreco.2010.07.054.

(10)   Niinemets, Ü.; Kännaste, A.; Copolovici, L. Quantitative Patterns between Plant Volatile Emissions Induced by Biotic Stresses and the Degree of Damage. *Front. Plant Sci.* **2013**, *4*. https://doi.org/10.3389/fpls.2013.00262.

(11)   Holopainen, J. K.; Gershenzon, J. Multiple Stress Factors and the Emission of Plant VOCs. *Trends in Plant Science* **2010**, *15* (3), 176–184. https://doi.org/10.1016/j.tplants.2010.01.006.

(12)   Yuan, J. S.; Himanen, S. J.; Holopainen, J. K.; Chen, F.; Stewart, C. N. Smelling Global Climate Change: Mitigation of Function for Plant Volatile Organic Compounds. *Trends in Ecology & Evolution* **2009**, *24* (6), 323–331. https://doi.org/10.1016/j.tree.2009.01.012.

(13)   Boyd, M. A.; Berner, L. T.; Doak, P.; Goetz, S.; Rogers, B.; Wagner, D.; Walker, X.; Mack, M. C. Impacts of Climate and Insect Herbivory on Productivity and Physiology of Trembling Aspen (Populus Tremuloides) in Alaskan Boreal Forests. *Environ. Res. Lett.* **2019**. https://doi.org/10.1088/1748-9326/ab215f.

(14)   Pureswaran, D. S.; Grandpré, L. D.; Paré, D.; Taylor, A.; Barrette, M.; Morin, H.; Régnière, J.;
         Kneeshaw, D. D. Climate-Induced Changes in Host Tree–Insect Phenology May Drive Ecological
         State-Shift in Boreal Forests. *Ecology* **2015**, *96* (6), 1480–1491. https://doi.org/10.1890/13-
         2366.1.

(15)   Chen, L.; Huang, J.-G.; Dawson, A.; Zhai, L.; Stadt, K. J.; Comeau, P. G.; Whitehouse, C.
         Contributions of Insects and Droughts to Growth Decline of Trembling Aspen Mixed Boreal Forest
         of Western Canada. *Global Change Biology* **2018**, *24* (2), 655–667.
         https://doi.org/10.1111/gcb.13855.

(16)   Guenther, A. B.; Jiang, X.; Heald, C. L.; Sakulyanontvittaya, T.; Duhl, T.; Emmons, L. K.; Wang, X.
         The Model of Emissions of Gases and Aerosols from Nature Version 2.1 (MEGAN2.1): An
         Extended and Updated Framework for Modeling Biogenic Emissions. *Geosci. Model Dev.* **2012**, *5*
         (6), 1471–1492. https://doi.org/10.5194/gmd-5-1471-2012.

(17)   Faiola, C. L.; Buchholz, A.; Kari, E.; Yli-Pirilä, P.; Holopainen, J. K.; Kivimäenpää, M.; Miettinen, P.;
         Worsnop, D. R.; Lehtinen, K. E. J.; Guenther, A. B.; et al. Terpene Composition Complexity
         Controls Secondary Organic Aerosol Yields from Scots Pine Volatile Emissions. *Scientific Reports*
         2018, *8* (1), 3053. https://doi.org/10.1038/s41598-018-21045-1.

(18)   Blande, J. D.; Korjus, M.; Holopainen, J. K. Foliar Methyl Salicylate Emissions Indicate Prolonged
         Aphid Infestation on Silver Birch and Black Alder. *Tree Physiol* **2010**, *30* (3), 404–416.
         https://doi.org/10.1093/treephys/tpp124.

(19)   Blande, J. D.; Turunen, K.; Holopainen, J. K. Pine Weevil Feeding on Norway Spruce Bark Has a
         Stronger Impact on Needle VOC Emissions than Enhanced Ultraviolet-B Radiation. *Environmental
         Pollution* **2009**, *157* (1), 174–180. https://doi.org/10.1016/j.envpol.2008.07.007.

(20)   Blande, J. D.; Tiiva, P.; Oksanen, E.; Holopainen, J. K. Emission of Herbivore-Induced Volatile
         Terpenoids from Two Hybrid Aspen (Populus Tremula×tremuloides) Clones under Ambient and
         Elevated Ozone Concentrations in the Field. *Global Change Biology* **2007**, *13* (12), 2538–2550.
         https://doi.org/10.1111/j.1365-2486.2007.01453.x.

(21)   Ghimire, R. P.; Markkanen, J. M.; Kivimäenpää, M.; Lyytikäinen-Saarenmaa, P.; Holopainen, J. K.
         Needle Removal by Pine Sawfly Larvae Increases Branch-Level VOC Emissions and Reduces
         Below-Ground Emissions of Scots Pine. *Environ. Sci. Technol.* **2013**, *47* (9), 4325–4332.
         https://doi.org/10.1021/es4006064.

(22)   Ghimire, R. P.; Kivimäenpää, M.; Blomqvist, M.; Holopainen, T.; Lyytikäinen-Saarenmaa, P.;
         Holopainen, J. K. Effect of Bark Beetle (Ips Typographus L.) Attack on Bark VOC Emissions of
         Norway Spruce (Picea Abies Karst.) Trees. *Atmospheric Environment* **2016**, *126*, 145–152.
         https://doi.org/10.1016/j.atmosenv.2015.11.049.

(23)   Ghimire, R. P.; Kivimäenpää, M.; Kasurinen, A.; Häikiö, E.; Holopainen, T.; Holopainen, J. K.
         Herbivore-Induced BVOC Emissions of Scots Pine under Warming, Elevated Ozone and Increased
         Nitrogen Availability in an Open-Field Exposure. *Agricultural and Forest Meteorology* **2017**, *242*,
         21–32. https://doi.org/10.1016/j.agrformet.2017.04.008.

(24)   Heijari, J.; Blande, J. D.; Holopainen, J. K. Feeding of Large Pine Weevil on Scots Pine Stem
         Triggers Localised Bark and Systemic Shoot Emission of Volatile Organic Compounds.
         Environmental and Experimental Botany **2011**, *71* (3), 390–398.
         https://doi.org/10.1016/j.envexpbot.2011.02.008.

(25)   Maja, M. M.; Kasurinen, A.; Yli-Pirilä, P.; Joutsensaari, J.; Klemola, T.; Holopainen, T.; Holopainen,
         J. K. Contrasting Responses of Silver Birch VOC Emissions to Short- and Long-Term Herbivory. *Tree
         Physiol* **2014**, *34* (3), 241–252. https://doi.org/10.1093/treephys/tpt127.

(26)   Yli-Pirilä, P.; Copolovici, L.; Kännaste, A.; Noe, S.; Blande, J. D.; Mikkonen, S.; Klemola, T.;
         Pulkkinen, J.; Virtanen, A.; Laaksonen, A.; et al. Herbivory by an Outbreaking Moth Increases
         Emissions of Biogenic Volatiles and Leads to Enhanced Secondary Organic Aerosol Formation

Capacity. *Environ. Sci. Technol.* **2016**, *50* (21), 11501–11510.
https://doi.org/10.1021/acs.est.6b02800.

(27)   Faiola, C. L.; Jobson, B. T.; VanReken, T. M. Impacts of Simulated Herbivory on Volatile Organic
Compound Emission Profiles from Coniferous Plants. *Biogeosciences* **2015**, *12* (2), 527–547.
https://doi.org/10.5194/bg-12-527-2015.

(28)   Berg, E. E.; David Henry, J.; Fastie, C. L.; De Volder, A. D.; Matsuoka, S. M. Spruce Beetle
Outbreaks on the Kenai Peninsula, Alaska, and Kluane National Park and Reserve, Yukon
Territory: Relationship to Summer Temperatures and Regional Differences in Disturbance
Regimes. *Forest Ecology and Management* **2006**, *227* (3), 219–232.
https://doi.org/10.1016/j.foreco.2006.02.038.

(29)   Ammunét, T.; Kaukoranta, T.; Saikkonen, K.; Repo, T.; Klemola, T. Invading and Resident
Defoliators in a Changing Climate: Cold Tolerance and Predictions Concerning Extreme Winter
Cold as a Range-Limiting Factor. *Ecological Entomology* **2012**, *37* (3), 212–220.
https://doi.org/10.1111/j.1365-2311.2012.01358.x.

(30)   Bale, J. S.; Masters, G. J.; Hodkinson, I. D.; Awmack, C.; Bezemer, T. M.; Brown, V. K.; Butterfield,
J.; Buse, A.; Coulson, J. C.; Farrar, J.; et al. Herbivory in Global Climate Change Research: Direct
Effects of Rising Temperature on Insect Herbivores. *Global Change Biology* **2002**, *8* (1), 1–16.
https://doi.org/10.1046/j.1365-2486.2002.00451.x.

(31)   Food and Agriculture Organization of the United Nations. *FAO's Work on Climate Change: United
Nations Climate Change Conference 2017*; 2017.

(32)   Bergström, R.; Hallquist, M.; Simpson, D.; Wildt, J.; Mentel, T. F. Biotic Stress: A Significant
Contributor to Organic Aerosol in Europe? *Atmos. Chem. Phys.* **2014**, *14* (24), 13643–13660.
https://doi.org/10.5194/acp-14-13643-2014.

(33)   Joutsensaari, J.; Yli-Pirilä, P.; Korhonen, H.; Arola, A.; Blande, J. D.; Heijari, J.; Kivimäenpää, M.;
Mikkonen, S.; Hao, L.; Miettinen, P.; et al. Biotic Stress Accelerates Formation of Climate-Relevant
Aerosols in Boreal Forests. *Atmos. Chem. Phys.* **2015**, *15* (21), 12139–12157.
https://doi.org/10.5194/acp-15-12139-2015.

(34)   Lang-Yona, N.; Rudich, Y.; Mentel, T. F.; Bohne, A.; Buchholz, A.; Kiendler-Scharr, A.; Kleist, E.;
Spindler, C.; Tillmann, R.; Wildt, J. The Chemical and Microphysical Properties of Secondary
Organic Aerosols from Holm Oak Emissions. *Atmospheric Chemistry and Physics* **2010**, *10* (15),
7253–7265. https://doi.org/10.5194/acp-10-7253-2010.

(35)   Mentel, Th. F.; Kleist, E.; Andres, S.; Dal Maso, M.; Hohaus, T.; Kiendler-Scharr, A.; Rudich, Y.;
Springer, M.; Tillmann, R.; Uerlings, R.; et al. Secondary Aerosol Formation from Stress-Induced
Biogenic Emissions and Possible Climate Feedbacks. *Atmos. Chem. Phys.* **2013**, *13* (17), 8755–
8770. https://doi.org/10.5194/acp-13-8755-2013.

(36)   Zhao, D. F.; Buchholz, A.; Tillmann, R.; Kleist, E.; Wu, C.; Rubach, F.; Kiendler-Scharr, A.; Rudich, Y.;
Wildt, J.; Mentel, T. F. Environmental Conditions Regulate the Impact of Plants on Cloud
Formation. *Nature Communications* **2017**, *8*, 14067. https://doi.org/10.1038/ncomms14067.

(37)   Mutzel, A.; Rodigast, M.; Iinuma, Y.; Böge, O.; Herrmann, H. Monoterpene SOA – Contribution of
First-Generation Oxidation Products to Formation and Chemical Composition. *Atmospheric
Environment* **2016**, *130*, 136–144. https://doi.org/10.1016/j.atmosenv.2015.10.080.

(38)   Hämet-Ahti, L.; Palmén, A.; Alanko, P.; Tigerstedt, P. M. A. *Woody Flora of Finland*; University
Press: Helsinki, 1992.

(39)   Peltola, A. Finnish Statistical Yearbook of Forestry 2014. Finnish Forest Research Institute,
Tampere. **2014**.

(40)   Ortega, J.; Helmig, D. Approaches for Quantifying Reactive and Low-Volatility Biogenic Organic
Compound Emissions by Vegetation Enclosure Techniques – Part A. *Chemosphere* **2008**, *72* (3),
343–364. https://doi.org/10.1016/j.chemosphere.2007.11.020.

(41) Helmig, D.; Ortega, J.; Guenther, A.; Herrick, J. D.; Geron, C. Sesquiterpene Emissions from Loblolly Pine and Their Potential Contribution to Biogenic Aerosol Formation in the Southeastern US. *Atmospheric Environment* **2006**, *40* (22), 4150–4157. https://doi.org/10.1016/j.atmosenv.2006.02.035.

(42) Mentel, T. F.; Springer, M.; Ehn, M.; Kleist, E.; Pullinen, I.; Kurtén, T.; Rissanen, M.; Wahner, A.; Wildt, J. Formation of Highly Oxidized Multifunctional Compounds: Autoxidation of Peroxy Radicals Formed in the Ozonolysis of Alkenes – Deduced from Structure–Product Relationships. *Atmospheric Chemistry and Physics* **2015**, *15* (12), 6745–6765. https://doi.org/10.5194/acp-15-6745-2015.

(43) Hansel, A.; Jordan, A.; Holzinger, R.; Prazeller, P.; Vogel, W.; Lindinger, W. Proton Transfer Reaction Mass Spectrometry: On-Line Trace Gas Analysis at the Ppb Level. *International Journal of Mass Spectrometry and Ion Processes* **1995**, *149–150*, 609–619. https://doi.org/10.1016/0168-1176(95)04294-U.

(44) Lindinger, W.; Jordan, A. Proton-Transfer-Reaction Mass Spectrometry (PTR–MS): On-Line Monitoring of Volatile Organic Compounds at Pptv Levels. *Chem. Soc. Rev.* **1998**, *27* (5), 347–375. https://doi.org/10.1039/A827347Z.

(45) Blake, R. S.; Monks, P. S.; Ellis, A. M. Proton-Transfer Reaction Mass Spectrometry. *Chem. Rev.* **2009**, *109* (3), 861–896. https://doi.org/10.1021/cr800364q.

(46) Jordan, A.; Haidacher, S.; Hanel, G.; Hartungen, E.; Märk, L.; Seehauser, H.; Schottkowsky, R.; Sulzer, P.; Märk, T. D. A High Resolution and High Sensitivity Proton-Transfer-Reaction Time-of-Flight Mass Spectrometer (PTR-TOF-MS). *International Journal of Mass Spectrometry* **2009**, *286* (2), 122–128. https://doi.org/10.1016/j.ijms.2009.07.005.

(47) Kari, E.; Miettinen, P.; Yli-Pirilä, P.; Virtanen, A.; Faiola, C. L. PTR-ToF-MS Product Ion Distributions and Humidity-Dependence of Biogenic Volatile Organic Compounds. *International Journal of Mass Spectrometry* **2018**, *430*, 87–97. https://doi.org/10.1016/j.ijms.2018.05.003.

(48) Kari, E.; Faiola, C. L.; Isokääntä, S.; Miettinen, P.; Yli-Pirilä, P.; Buchholz, A.; Kivimäenpää, M.; Mikkonen, S.; Holopainen, J. K.; Virtanen, A. Time-Resolved Characterization of Biotic Stress Emissions from Scots Pines Being Fed upon by Pine Weevil by Means of PTR-ToF-MS. *Bor. Env. Res.* **2019**, *24*, 25–49.

(49) Junninen, H.; Ehn, M.; Petäjä, T.; Luosujärvi, L.; Kotiaho, T.; Kostiainen, R.; Rohner, U.; Gonin, M.; Fuhrer, K.; Kulmala, M.; et al. A High-Resolution Mass Spectrometer to Measure Atmospheric Ion Composition. *Atmospheric Measurement Techniques* **2010**, *3* (4), 1039–1053. https://doi.org/10.5194/amt-3-1039-2010.

(50) Veres, P.; Roberts, J. M.; Warneke, C.; Welsh-Bon, D.; Zahniser, M.; Herndon, S.; Fall, R.; de Gouw, J. Development of Negative-Ion Proton-Transfer Chemical-Ionization Mass Spectrometry (NI-PT-CIMS) for the Measurement of Gas-Phase Organic Acids in the Atmosphere. *International Journal of Mass Spectrometry* **2008**, *274* (1), 48–55. https://doi.org/10.1016/j.ijms.2008.04.032.

(51) Bertram, T. H.; Kimmel, J. R.; Crisp, T. A.; Ryder, O. S.; Yatavelli, R. L. N.; Thornton, J. A.; Cubison, M. J.; Gonin, M.; Worsnop, D. R. A Field-Deployable, Chemical Ionization Time-of-Flight Mass Spectrometer. *Atmospheric Measurement Techniques* **2011**, *4* (7), 1471–1479. https://doi.org/10.5194/amt-4-1471-2011.

(52) Aljawhary, D.; Lee, A. K. Y.; Abbatt, J. P. D. High-Resolution Chemical Ionization Mass Spectrometry (ToF-CIMS): Application to Study SOA Composition and Processing. *Atmospheric Measurement Techniques* **2013**, *6* (11), 3211–3224. https://doi.org/10.5194/amt-6-3211-2013.

(53) Brophy, P.; Farmer, D. K. Clustering, Methodology, and Mechanistic Insights into Acetate Chemical Ionization Using High-Resolution Time-of-Flight Mass Spectrometry. *Atmospheric Measurement Techniques* **2016**, *9* (8), 3969–3986. https://doi.org/10.5194/amt-9-3969-2016.
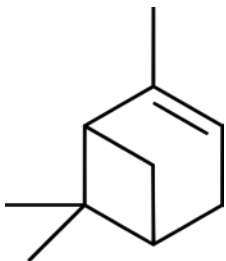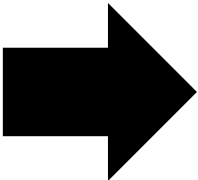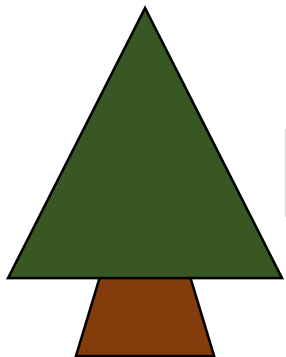
(54) DeCarlo, P. F.; Kimmel, J. R.; Trimborn, A.; Northway, M. J.; Jayne, J. T.; Aiken, A. C.; Gonin, M.; Fuhrer, K.; Horvath, T.; Docherty, K. S.; et al. Field-Deployable, High-Resolution, Time-of-Flight Aerosol Mass Spectrometer. *Anal. Chem.* **2006**, *78* (24), 8281–8289. https://doi.org/10.1021/ac061249n.

(55) Canagaratna, M. R.; Jayne, J. T.; Jimenez, J. L.; Allan, J. D.; Alfarra, M. R.; Zhang, Q.; Onasch, T. B.; Drewnick, F.; Coe, H.; Middlebrook, A.; et al. Chemical and Microphysical Characterization of Ambient Aerosols with the Aerodyne Aerosol Mass Spectrometer. *Mass Spectrometry Reviews* **2007**, *26* (2), 185–222. https://doi.org/10.1002/mas.20115.

(56) VanReken, T.   M; Greenberg, J.   P; Harley, P.   C; Guenther, A.   B; Smith, J.   N. Direct Measurement of Particle Formation and Growth from the Oxidation of Biogenic Emissions. *Atmospheric Chemistry and Physics* **2006**, *6* (12), 4403–4413. https://doi.org/10.5194/acp-6-4403-2006.

(57) Zhang, X.; Schwantes, R. H.; McVay, R. C.; Lignell, H.; Coggon, M. M.; Flagan, R. C.; Seinfeld, J. H. Vapor Wall Deposition in Teflon Chambers. *Atmospheric Chemistry and Physics* **2015**, *15* (8), 4197–4214. https://doi.org/10.5194/acp-15-4197-2015.

(58) Loza, C. L.; Chan, A. W. H.; Galloway, M. M.; Keutsch, F. N.; Flagan, R. C.; Seinfeld, J. H. Characterization of Vapor Wall Loss in Laboratory Chambers. *Environ. Sci. Technol.* **2010**, *44* (13), 5074–5078. https://doi.org/10.1021/es100727v.

(59) McVay, R. C.; Cappa, C. D.; Seinfeld, J. H. Vapor–Wall Deposition in Chambers: Theoretical Considerations. *Environ. Sci. Technol.* **2014**, *48* (17), 10251–10258. https://doi.org/10.1021/es502170j.

(60) Nah, T.; McVay, R. C.; Zhang, X.; Boyd, C. M.; Seinfeld, J. H.; Ng, N. L. Influence of Seed Aerosol Surface Area and Oxidation Rate on Vapor Wall Deposition and SOA Mass Yields: A Case Study with α-Pinene Ozonolysis. *Atmospheric Chemistry and Physics* **2016**, *16* (14), 9361–9379. https://doi.org/10.5194/acp-16-9361-2016.

(61) Zhang, X.; Cappa, C. D.; Jathar, S. H.; McVay, R. C.; Ensberg, J. J.; Kleeman, M. J.; Seinfeld, J. H. Influence of Vapor Wall Loss in Laboratory Chambers on Yields of Secondary Organic Aerosol. *PNAS* **2014**, *111* (16), 5802–5807. https://doi.org/10.1073/pnas.1404727111.

(62) Nah, T.; McVay, R. C.; Pierce, J. R.; Seinfeld, J. H.; Ng, N. L. Constraining Uncertainties in Particle-Wall Deposition Correction during SOA Formation in Chamber Experiments. *Atmospheric Chemistry and Physics* **2017**, *17* (3), 2297–2310. https://doi.org/10.5194/acp-17-2297-2017.

(63) Trump, E. R.; Epstein, S. A.; Riipinen, I.; Donahue, N. M. Wall Effects in Smog Chamber Experiments: A Model Study. *Aerosol Science and Technology* **2016**, *50* (11), 1180–1200. https://doi.org/10.1080/02786826.2016.1232858.

(64) Huang, Y.; Zhao, R.; Charan, S. M.; Kenseth, C. M.; Zhang, X.; Seinfeld, J. H. Unified Theory of Vapor–Wall Mass Transport in Teflon-Walled Environmental Chambers. *Environ. Sci. Technol.* **2018**, *52* (4), 2134–2142. https://doi.org/10.1021/acs.est.7b05575.

(65) Bian, Q.; May, A. A.; Kreidenweis, S. M.; Pierce, J. R. Investigation of Particle and Vapor Wall-Loss Effects on Controlled Wood-Smoke Smog-Chamber Experiments. *Atmospheric Chemistry and Physics* **2015**, *15* (19), 11027–11045. https://doi.org/10.5194/acp-15-11027-2015.

(66) Ye, P.; Ding, X.; Hakala, J.; Hofbauer, V.; Robinson, E. S.; Donahue, N. M. Vapor Wall Loss of Semi-Volatile Organic Compounds in a Teflon Chamber. *Aerosol Science and Technology* **2016**, *50* (8), 822–834. https://doi.org/10.1080/02786826.2016.1195905.

(67) Krechmer, J. E.; Pagonis, D.; Ziemann, P. J.; Jimenez, J. L. Quantification of Gas-Wall Partitioning in Teflon Environmental Chambers Using Rapid Bursts of Low-Volatility Oxidized Species Generated in Situ. *Environ. Sci. Technol.* **2016**, *50* (11), 5757–5765. https://doi.org/10.1021/acs.est.6b00606.

(68) Matsunaga, A.; Ziemann ‡, P. J. Gas-Wall Partitioning of Organic Compounds in a Teflon Film Chamber and Potential Effects on Reaction Product and Aerosol Yield Measurements. *Aerosol Science and Technology* **2010**, *44* (10), 881–892. https://doi.org/10.1080/02786826.2010.501044.

(69) Barmet, P.; Dommen, J.; DeCarlo, P. F.; Tritscher, T.; Praplan, A. P.; Platt, S. M.; Prévôt, A. S. H.; Donahue, N. M.; Baltensperger, U. OH Clock Determination by Proton Transfer Reaction Mass Spectrometry at an Environmental Chamber. *Atmospheric Measurement Techniques* **2012**, *5* (3), 647–656. https://doi.org/10.5194/amt-5-647-2012.

(70) Li, Y.; Pöschl, U.; Shiraiwa, M. Molecular Corridors and Parameterizations of Volatility in the Chemical Evolution of Organic Aerosols. *Atmospheric Chemistry and Physics* **2016**, *16* (5), 3327–3344. https://doi.org/10.5194/acp-16-3327-2016.

(71) Ye, J.; Jiang, Y.; Veromann-Jürgenson, L.-L.; Niinemets, Ü. Petiole Gall Aphid (Pemphigus Spyrothecae) Infestation of Populus × Petrovskiana Leaves Alters Foliage Photosynthetic Characteristics and Leads to Enhanced Emissions of Both Constitutive and Stress-Induced Volatiles. *Trees* **2019**, *33* (1), 37–51. https://doi.org/10.1007/s00468-018-1756-2.

(72) Pickett, J. A.; Allemann, R. K.; Birkett, M. A. The Semiochemistry of Aphids. *Nat. Prod. Rep.* **2013**, *30* (10), 1277–1283. https://doi.org/10.1039/C3NP70036D.

(73) Pezet, J.; Elkinton, J.; Gomez, S.; Mckenzie, E. A.; Lavine, M.; Preisser, E. Hemlock Woolly Adelgid and Elongate Hemlock Scale Induce Changes in Foliar and Twig Volatiles of Eastern Hemlock. *J Chem Ecol* **2013**, *39* (8), 1090–1100. https://doi.org/10.1007/s10886-013-0300-5.

(74) Kleist, E.; Mentel, T. F.; Andres, S.; Bohne, A.; Folkers, A.; Kiendler-Scharr, A.; Rudich, Y.; Springer, M.; Tillmann, R.; Wildt, J. Irreversible Impacts of Heat on the Emissions of Monoterpenes, Sesquiterpenes, Phenolic BVOC and Green Leaf Volatiles from Several Tree Species. *Biogeosciences* **2012**, *9* (12), 5111–5123. https://doi.org/10.5194/bg-9-5111-2012.

(75) Joó, É.; Dewulf, J.; Amelynck, C.; Schoon, N.; Pokorska, O.; Šimpraga, M.; Steppe, K.; Aubinet, M.; Van Langenhove, H. Constitutive versus Heat and Biotic Stress Induced BVOC Emissions in Pseudotsuga Menziesii. *Atmospheric Environment* **2011**, *45* (22), 3655–3662. https://doi.org/10.1016/j.atmosenv.2011.04.048.

(76) Brown, R. L.; El-Sayed, A. M.; Unelius, C. R.; Beggs, J. R.; Suckling, D. M. Invasive Vespula Wasps Utilize Kairomones to Exploit Honeydew Produced by Sooty Scale Insects, Ultracoelostoma. *J Chem Ecol* **2015**, *41* (11), 1018–1027. https://doi.org/10.1007/s10886-015-0635-1.

(77) Azeem, M.; Rajarao, G. K.; Terenius, O.; Nordlander, G.; Nordenhem, H.; Nagahama, K.; Norin, E.; Borg-Karlson, A. K. A Fungal Metabolite Masks the Host Plant Odor for the Pine Weevil (Hylobius Abietis). *Fungal Ecology* **2015**, *13*, 103–111. https://doi.org/10.1016/j.funeco.2014.08.009.

(78) Jiang, Y.; Ye, J.; Veromann, L.-L.; Niinemets, Ü. Scaling of Photosynthesis and Constitutive and Induced Volatile Emissions with Severity of Leaf Infection by Rust Fungus (Melampsora Larici-Populina) in Populus Balsamifera Var. Suaveolens. *Tree Physiol* **2016**, *36* (7), 856–872. https://doi.org/10.1093/treephys/tpw035.

(79) Pankow, J. F. An Absorption Model of Gas/Particle Partitioning of Organic Compounds in the Atmosphere. *Atmospheric Environment* **1994**, *28* (2), 185–188. https://doi.org/10.1016/1352-2310(94)90093-0.

(80) Odum, J. R.; Hoffmann, T.; Bowman, F.; Collins, D.; Flagan, R. C.; Seinfeld, J. H. Gas/Particle Partitioning and Secondary Organic Aerosol Yields. *Environ. Sci. Technol.* **1996**, *30* (8), 2580–2585. https://doi.org/10.1021/es950943+.

(81) Pathak, R. K.; Presto, A. A.; Lane, T. E.; Stanier, C. O.; Donahue, N. M.; Pandis, S. N. Ozonolysis of α-Pinene: Parameterization of Secondary Organic Aerosol Mass Fraction. *Atmospheric Chemistry and Physics* **2007**, *7* (14), 3811–3821. https://doi.org/10.5194/acp-7-3811-2007.

(82) Lee, A.; Goldstein, A. H.; Kroll, J. H.; Ng, N. L.; Varutbangkul, V.; Flagan, R. C.; Seinfeld, J. H. Gas-Phase Products and Secondary Aerosol Yields from the Photooxidation of 16 Different Terpenes.
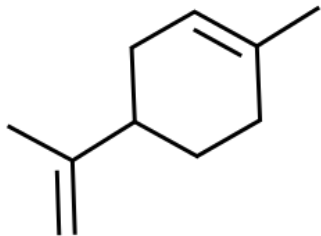
Journal of Geophysical Research: Atmospheres 111 (D17).
https://doi.org/10.1029/2006JD007050.

(83)   Lee, A.; Goldstein, A. H.; Keywood, M. D.; Gao, S.; Varutbangkul, V.; Bahreini, R.; Ng, N. L.; Flagan, R. C.; Seinfeld, J. H. Gas-Phase Products and Secondary Aerosol Yields from the Ozonolysis of Ten Different Terpenes. *Journal of Geophysical Research: Atmospheres 111* (D7). https://doi.org/10.1029/2005JD006437.

(84)   Ng, N. L.; Chhabra, P. S.; Chan, A. W. H.; Surratt, J. D.; Kroll, J. H.; Kwan, A. J.; McCabe, D. C.; Wennberg, P. O.; Sorooshian, A.; Murphy, S. M.; et al. Effect of NOx Level on Secondary Organic Aerosol (SOA) Formation from the Photooxidation of Terpenes. *Atmos. Chem. Phys.* **2007**, *7* (19), 5159–5174. https://doi.org/10.5194/acp-7-5159-2007.

(85)   Ng, N. L.; Kroll, J. H.; Keywood, M. D.; Bahreini, R.; Varutbangkul, V.; Flagan, R. C.; Seinfeld, J. H.; Lee, A.; Goldstein, A. H. Contribution of First- versus Second-Generation Products to Secondary Organic Aerosols Formed in the Oxidation of Biogenic Hydrocarbons. *Environ. Sci. Technol.* **2006**, *40* (7), 2283–2297. https://doi.org/10.1021/es052269u.

(86)   Eddingsaas, N. C.; Loza, C. L.; Yee, L. D.; Chan, M.; Schilling, K. A.; Chhabra, P. S.; Seinfeld, J. H.; Wennberg, P. O. α-Pinene Photooxidation under Controlled Chemical Conditions – Part 2: SOA Yield and Composition in Low- and High-NOx Environments. *Atmos. Chem. Phys.* **2012**, *12* (16), 7413–7427. https://doi.org/10.5194/acp-12-7413-2012.

(87)   Zhao, D.; Schmitt, S. H.; Wang, M.; Acir, I.-H.; Tillmann, R.; Tan, Z.; Novelli, A.; Fuchs, H.; Pullinen, I.; Wegener, R.; et al. Effects of NO_x and SO_2 on the Secondary Organic Aerosol Formation from Photooxidation of α-Pinene and Limonene. *Atmospheric Chemistry and Physics* **2018**, *18* (3), 1611–1628. https://doi.org/10.5194/acp-18-1611-2018.

(88)   Zhao, D. F.; Kaminski, M.; Schlag, P.; Fuchs, H.; Acir, I.-H.; Bohn, B.; Häseler, R.; Kiendler-Scharr, A.; Rohrer, F.; Tillmann, R.; et al. Secondary Organic Aerosol Formation from Hydroxyl Radical Oxidation and Ozonolysis of Monoterpenes. *Atmospheric Chemistry and Physics* **2015**, *15* (2), 991–1012. https://doi.org/10.5194/acp-15-991-2015.

(89)   Canagaratna, M. R.; Jimenez, J. L.; Kroll, J. H.; Chen, Q.; Kessler, S. H.; Massoli, P.; Hildebrandt Ruiz, L.; Fortner, E.; Williams, L. R.; Wilson, K. R.; et al. Elemental Ratio Measurements of Organic Compounds Using Aerosol Mass Spectrometry: Characterization, Improved Calibration, and Implications. *Atmospheric Chemistry and Physics* **2015**, *15* (1), 253–272. https://doi.org/10.5194/acp-15-253-2015.

(90)   Ng, N. L.; Canagaratna, M. R.; Zhang, Q.; Jimenez, J. L.; Tian, J.; Ulbrich, I. M.; Kroll, J. H.; Docherty, K. S.; Chhabra, P. S.; Bahreini, R.; et al. Organic Aerosol Components Observed in Northern Hemispheric Datasets from Aerosol Mass Spectrometry. *Atmospheric Chemistry and Physics* **2010**, *10* (10), 4625–4641. https://doi.org/10.5194/acp-10-4625-2010.

(91)   Kroll, J. H.; Donahue, N. M.; Jimenez, J. L.; Kessler, S. H.; Canagaratna, M. R.; Wilson, K. R.; Altieri, K. E.; Mazzoleni, L. R.; Wozniak, A. S.; Bluhm, H. Carbon Oxidation State as a Metric for Describing the Chemistry of Atmospheric Organic Aerosol. *Nature Chemistry* **2011**, *3* (2), 133. https://doi.org/10.1038/nchem.948.

(92)   Donahue, N. M.; Robinson, A. L.; Stanier, C. O.; Pandis, S. N. Coupled Partitioning, Dilution, and Chemical Aging of Semivolatile Organics. *Environ. Sci. Technol.* **2006**, *40* (8), 2635–2643. https://doi.org/10.1021/es052297c.

(93)   Hao, L.; Garmash, O.; Ehn, M.; Miettinen, P.; Massoli, P.; Mikkonen, S.; Jokinen, T.; Roldin, P.; Aalto, P.; Yli-Juuti, T.; et al. Combined Effects of Boundary Layer Dynamics and Atmospheric Chemistry on Aerosol Composition during New Particle Formation Periods. *Atmospheric Chemistry and Physics* **2018**, *18* (23), 17705–17716. https://doi.org/10.5194/acp-18-17705-2018.

(94)   Chhabra, P. S.; Lambe, A. T.; Canagaratna, M. R.; Stark, H.; Jayne, J. T.; Onasch, T. B.; Davidovits, P.; Kimmel, J. R.; Worsnop, D. R. Application of High-Resolution Time-of-Flight Chemical

Ionization Mass Spectrometry Measurements to Estimate Volatility Distributions of α-Pinene and Naphthalene Oxidation Products. *Atmospheric Measurement Techniques* **2015**, *8* (1), 1–18. https://doi.org/10.5194/amt-8-1-2015.

(95)   McFiggans, G.; Mentel, T. F.; Wildt, J.; Pullinen, I.; Kang, S.; Kleist, E.; Schmitt, S.; Springer, M.; Tillmann, R.; Wu, C.; et al. Secondary Organic Aerosol Reduced by Mixture of Atmospheric Vapours. *Nature* **2019**, *565* (7741), 587. https://doi.org/10.1038/s41586-018-0871-y.

(96)   Wang, S.; Wu, R.; Berndt, T.; Ehn, M.; Wang, L. Formation of Highly Oxidized Radicals and Multifunctional Products from the Atmospheric Oxidation of Alkylbenzenes. *Environ. Sci. Technol.* **2017**, *51* (15), 8442–8449. https://doi.org/10.1021/acs.est.7b02374.

(97)   Jaoui, M.; Lewandowski, M.; Docherty, K. S.; Corse, E. W.; Lonneman, W. A.; Offenberg, J. H.; Kleindienst, T. E. Photooxidation of Farnesene Mixtures in the Presence of NOx: Analysis of Reaction Products and Their Implication to Ambient PM2.5. *Atmospheric Environment* **2016**, *130*, 190–201. https://doi.org/10.1016/j.atmosenv.2015.10.091.

(98)   Jaoui, M.; Kleindienst, T. E.; Docherty, K. S.; Lewandowski, M.; Offenberg, J. H. Secondary Organic Aerosol Formation from the Oxidation of a Series of Sesquiterpenes: α-Cedrene, β-Caryophyllene, α-Humulene and α-Farnesene with O3, OH and NO3 Radicals. *Environ. Chem.* **2013**, *10* (3), 178–193. https://doi.org/10.1071/EN13025.

(99)   Misztal, P. K.; Hewitt, C. N.; Wildt, J.; Blande, J. D.; Eller, A. S. D.; Fares, S.; Gentner, D. R.; Gilman, J. B.; Graus, M.; Greenberg, J.; et al. Atmospheric Benzenoid Emissions from Plants Rival Those from Fo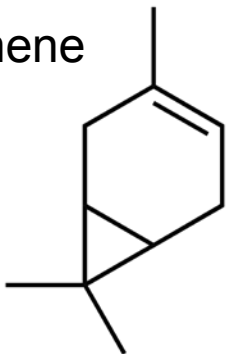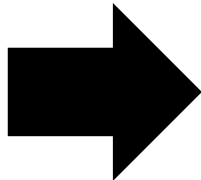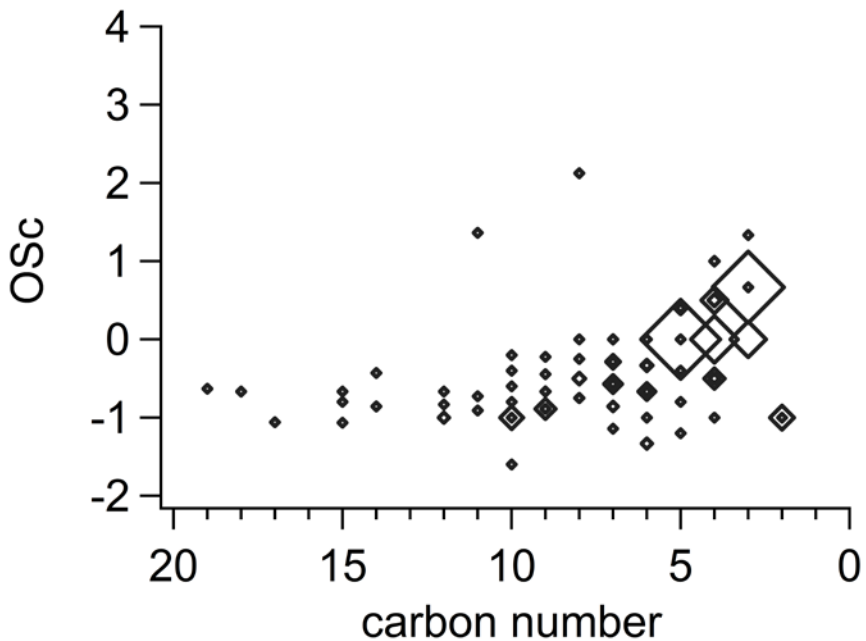ssil Fuels. *Scientific Reports* **2015**, *5*, 12064. https://doi.org/10.1038/srep12064.